Shape Optimisation of Cold-formed Steel Framed Wall Studs with Sheathing Restraints

Yomal Dias, Mahen Mahendran*

Queensland University of Technology (QUT), Brisbane, QLD 4000, Australia

Abstract

The optimisation of the cross sectional geometry of cold-formed steel sections has been the subject of numerous past studies. These walls consist of intermittently placed cold-formed steel studs, lined most commonly with gypsum plasterboards. Experimental evidence has shown that the restraints provided by the wall sheathing can have a significant impact on the axial compression capacity of these wall studs. However, the optimisation studies of cold-formed steel wall studs, incorporating sheathing restraints into the analysis, have been limited despite their potential for useful outcomes. A shape optimisation study was therefore conducted using two stochastic search algorithms: Simulated annealing and the Genetic algorithm. The in-plane and out-of-plane sheathing restraints to wall studs, estimated based on full-scale axial compression test results, were incorporated into the analyses. Structurally superior alternatives to four lipped channel studs currently used in the industry, made using 1.15mm thick G500 steel, were found. The results revealed that by increasing the number of rollers used in the roll forming process to 6 or 8, significant enhancements in the structural efficiency could be obtained for the commonly used 4-roller lipped channel stud. Elimination of local buckling due to web segmentation, and distortional and minor-axis global buckling due to the provision of sheathing restraints were identified as the prime causes of strength enhancement.

Keywords: Shape optimisation; Cold-formed steel; Structural efficiency; Simulated annealing; Genetic algorithm

*Corresponding author.
Email address: m.mahendran@qut.edu.au (Mahen Mahendran)

1. Introduction

Shape optimisation of cold-formed steel sections aims at developing cold-formed steel (CFS) sections with superior structural efficiency and economy. Shape optimisation is typically approached as a minimisation problem, where search algorithms are employed to determine the "optimum solution" within a defined design space. A common methodology in determining the optimum solution is the minimisation of the cross sectional area (A_g) of the CFS section while maintaining a constant member capacity (N_c) [1, 2]. Alternatively, the optimum solution can be the one giving the highest member capacity for a constant cross sectional area [3, 4].

Over the past several decades, the problem of optimising basic cold-formed sections to develop superior ones has been addressed repeatedly. Seaburg and Salmon [1] used both direct search and gradient-based search algorithms to determine the minimum weight cross sections of hat-shaped sections. Tian and Lu [2] used a non-linear constrained optimisation procedure based on the sequential quadratic programming (SQP) algorithm to develop minimum weight solutions of CFS sections subjected to axial compression. Only lipped and un-lipped channel sections were considered in their analyses. A knowledge-based global optimisation scheme was developed by Liu et al. [4] employing a numerical implementation of the Direct Strength Method (DSM) for the objective function. Lee et al. [5] used genetic algorithms to identify optimum cross sections of CFS columns subjected to axial compression. Gilbert et al. [6] developed a self-shaping optimisation method using the Genetic algorithm (GA). The method was subsequently further extended to optimise CFS columns, and a set of rules was proposed to automatically obtain local and distortional buckling stresses using the Finite Strip Method (FSM) during the optimisation process [7]. Leng et al. [3] used three formal optimisation algorithms: the gradient-based steepest descent method, Genetic algorithm and Simulated annealing (SA) and found the latter two stochastic search methods to search the design space more comprehensively. The formulation of the objective function was done using the FSM for stability analysis and the DSM for the strength calculation. Their work was further extended subsequently to introduce geometric and manufacturing constraints in the optimisation algorithms [8].

A coupled framework was presented by [9] for element and structural level optimisation of CFS portal frames using GA. Optimisation studies of cold-formed steel channels have also been conducted using the Particle Swarm Optimisation (PSO) method by [10, 11]. Local-flexurabl interaction of optimised cold-formed steel columns was investigated subsequently using this method by [12]. The optimisation of CFS sections for maximum energy dissipation in uniaxial bending, targeting improved seismic performance, was conducted using the same method by [13]. Overall, there is continuous interest in the optimisation of cold-formed steel sections for various applications.

The objective of this study is to develop optimised alternative sections with superior structural efficiency to the basic light gauge steel-framed (LSF) wall studs currently used in the industry. Particular emphasis is given to incorporating the restraints provided by the wall sheathing to the studs in this optimisation process. While optimisation studies of LSF wall studs have been conducted before, none have incorporated the effects of sheathing restraints. Such effects were proven to bring significant enhancements to the axial compression capacities of the studs through full-scale axial compression tests in previous studies [14]. The web-stiffened stud used in these axial compression tests was an improved stud geometry determined from a spreadsheet-based preliminary optimisation study. A formal algorithm based robust optimisation scheme is expected to better search the design space and identify further optimised cross sections. This paper presents the details on the use of optimisation algorithms specifically addressing sheathed LSF wall studs and the resultant optimum stud geometries found. Finite element modelling was used to investigate the behaviour and capacity of LSF walls built using these optimised studs.

2. Formulation of the optimisation problem

2.1. Overview

Only mono-symmetric sections are considered in the analyses. The number of folds within the cross section geometry is considered as a primary design variable, governed by the number of rollers employed in the roll-forming process. Leng et al. [8] considered the number of rollers to vary between 4 and 12 in their optimisation studies. Based on the overall strip widths considered in this study, the number of rollers is considered to vary between 4 and 8. Other variables include individual element lengths and turn angles at each fold. The length of the steel stud is set as 3.0 m, in line with the previous full-scale LSF wall experiments conducted. An elastic modulus of 220 GPa and a yield strength of 610 MPa are considered in the analyses. These were found to be the mechanical properties of the tested web-stiffened studs through tensile coupon testing [14]. Optimised sections were found for four 1.15 mm thick basic LSF wall stud sections with different section depths currently used in the industry.

2.2. Mathematical formulation of the cross section

Fig. 1 shows the general definition of node numbers, element widths and turn angles for a conventional lipped channel section. The origin of the Cartesian coordinate system used in the definition of nodal coordinates is placed at node 1. Turn angles at each node are measured clockwise from the positive X-axis.

2.3. Simulation of sheathing restraints

A detailed explanation of the restraints provided to LSF wall studs by the sheathing was presented in [14]. It was stated that the provision of full in-plane translational restraints (k_x) and no rotational or out-of-plane translational restraints (k_y) is an acceptable basic representation of sheathed LSF wall studs (Fig. 1). Thus, the optimisation algorithm was run for CFS stud sections which have their flange mid node (nodes 3 and 7 in Fig. 1) fully restrained in the plane of the wall. This restraint was applied by fully restraining the translation degree of freedom in the X direction at these nodes. This could easily be done by setting the 'xdof' to zero in the CUFSM nodal definition. Different cases were considered in terms of the out-of-plane restraint (k_y) to show its influence on the optimisation process. These included the provision of 0 (No out-of-plane restraints), 10 and 20 N/mm k_y restraints. No rotational restraints (k_ϕ) were provided. This 0 - 20 N/mm k_y interval was determined based on the mobilised out-of-plane sheathing restraints calculated in [14].These out-of-plane restraints were defined as springs with translational degree of freedom in the out-of-plane direction (zdof) with appropriate 'kspring' values in CUFSM. Fig. 2 indicates the method of simulating these restraints in CUFSM and Abaqus.

2.4. Basic studs

Shown in Fig. 3 are the 1.15 mm thick LSF wall studs commonly used in the industry [15]. 1.15 mm thick steel was also used when fabricating the web-stiffened stud. The overall section depth of commercially available 1.15 mm thick studs varies between 64 mm and 150 mm, as shown in Table 1. The optimisation process is carried out on each of these basic sections to optimise their shape and enhance their structural efficiency. The minimum width of the flange of commercially available studs is usually 33.5 mm, as seen in Fig. 3. This is based on the 32 mm minimum flange width specified in the design standards [16] for studs intended to accommodate wall sheathing. The lengths of the two flanges differ slightly allowing them to be boxed together. For simplicity, the two flanges were considered to be of equal width and the minimum flange width was taken to be 35.5 mm. The standards also specify the minimum lip length to be taken as 5 mm [16].

Table 1 and Fig. 4 provide details of the four basic sections considered in this study. Each of these sections is optimised, and the results are categorised accordingly in the following sections. In addition to this, details about the web-stiffened stud used in previous studies [14] are also included, and its performance is compared against that of the optimised studs.

2.5. Depth constrained and unconstrained analyses

The standard LSF wall stud depths used in the industry are as shown in Table 1. To allow a greater degree of freedom to the optimisation process, analyses are first conducted without incorporating the strict necessity to maintain these standard depths. This exercise is expected to highlight the deficiencies of the basic sections used at present. The resulting stud sections are expected to be non-standard yet more beneficial in terms of performance. Secondly, optimisation is carried out enforcing the standard depth requirements. This exercise is expected to produce practically usable optimised sections that are superior to the basic sections while conforming to the standards set by the industry.

2.6. Formulation of the design variable vector

The following section details the formulation of the design variable vector for the 4-fold lipped channel section shown in Fig. 1. The original length vector comprises all the individual element lengths and is given by,

$$l_{Original} = \begin{bmatrix} l_1 & l_2 & l_3 & l_4 & l_5 & l_6 & l_7 & l_8 \end{bmatrix}$$

The turn angle vector is originally defined as,

$$\theta_{Original} = \begin{bmatrix} \theta_1 & \theta_2 & \theta_3 & \theta_4 & \theta_5 & \theta_6 & \theta_7 & \theta_8 \end{bmatrix}$$

Combining the original length and turn angle vectors formulates the original design variable vector as,

$$X_{Original} = \begin{bmatrix} l_1 & l_2 & l_3 & l_4 & l_5 & l_6 & l_7 & l_8 & \theta_1 & \theta_2 & \theta_3 & \theta_4 & \theta_5 & \theta_6 & \theta_7 & \theta_8 \end{bmatrix}$$

2.7. Reduction of the design variable vector

The number of variables in the original length and turn angle vectors can be reduced by considering the symmetry of the section and other geometric constraints such as the necessity of parallel flanges. This reduces the number of input variables and eliminates the necessity for additional constraints in the optimisation algorithm. Such improvements are found to aid the algorithm to perform its search for the global minimum more efficiently and effectively. During the analysis, the reduced design variable vector fed to the optimisation algorithm is redefined in each iteration in an expanded form, thus reintroducing the mirrored and constrained variables.

2.7.1. Reduction of the length vector

Using the symmetry condition, the element lengths of the top half of the cross section can be defined using those of the bottom half. Hence, the length vector for the lipped channel section shown in Fig. 1 can be reduced as,

$$l = \begin{bmatrix} l_1 & l_2 & l_3 & l_4 \end{bmatrix}$$

The optimisation is conducted for steel strips of given total widths. This can be introduced as a geometric constraint governing the choice of element lengths as,

$$\sum_{n=1}^{4} l_i = L/2$$

where L is the total width of the steel strip. Alternatively, this constraint can be used to reduce the number of input variables further by defining one of the element widths as the difference between $L/2$ and the total width of the rest of the plate elements. For instance, l_4 can be represented as,

$$l_4 = L/2 - \sum_{n=1}^{3} l_i$$

This latter method is used in this study. The sheathing restraints to the stud are usually specified at the mid-point of the flange in numerical studies. For this purpose, it is advantageous to have a node at the centre of the flange, raising the necessity for the following constraint.

$$l_2 = l_3$$

This constraint can be introduced as a linear equality constraint as,

$$l_2 - l_3 = 0$$

Alternatively, by defining the total length of the flange as l_f, and allocating $l_f/2$ for each of the flange elements, another design variable can be reduced as,

$$l_2 = l_3 = l_f/2$$

This latter method is found to improve the efficiency and the effectiveness of the search for the global minimum and is used in this study. The length vector of the lipped channel section can, therefore, be reduced to only two independent length variables as,

$$l_{Reduced} = \begin{bmatrix} l_1 & l_f \end{bmatrix}$$

Its expanded form, redefined in each iteration during the analysis, is given by,

$$l_{Expanded} = \begin{bmatrix} l_1 & l_f/2 & l_f/2 & (L/2 - l_1 - l_f) \end{bmatrix}$$

2.7.2. Reduction of the turn angle vector

As the turn angles of the top half of the section can be defined using those of the bottom half using the symmetry, θ_6 to θ_8 can be removed as independent variables from the turn angle vector. Node 5 in Fig. 1 is defined at mid-height of the web only to divide the cross section into two halves.

To make the flanges parallel and symmetric about the major axis of the section, the turn angles θ_2 and θ_3 require to be constrained to 180°. This can be achieved with the definition of two equality constraints as,

$$\theta_2 = 180$$

$$\theta_3 = 180$$

Alternatively, these can be treated as non-variables and removed from the original turn angle vector and reintroduced subsequently into the expanded version as,

$$\theta_{Reduced} = \begin{bmatrix} \theta_1 & \theta_4 \end{bmatrix}$$

$$\theta_{Expanded} = \begin{bmatrix} \theta_1 & 180 & 180 & \theta_4 \end{bmatrix}$$

This latter method is used in this study as it improves the efficiency and the effectiveness of the search algorithm. Furthermore, for a lipped channel section, θ_4 is known to be constant at 270°. Thus, the turn angle vector can be reduced to a single element vector as,

$$\theta_{Original} = \begin{bmatrix} \theta_1 \end{bmatrix}$$

and, θ_4 can be reintroduced in the expanded version as a constant of 270°as,

$$\theta_{Expanded} = \begin{bmatrix} \theta_1 & 180 & 180 & 270 \end{bmatrix}$$

Thus, for the lipped channel shown in Fig. 1, the reduced design variable vector is defined as,

$$X_{Reduced} = \begin{bmatrix} l_1 & l_f & \theta_1 \end{bmatrix}$$

It is subsequently expanded as,

$$X_{Expanded} = \begin{bmatrix} l_1 & l_f/2 & l_f/2 & (L/2 - l_1 - l_f) & \theta_1 & 180 & 180 & 270 \end{bmatrix}$$

The design variables for other cases are also defined using a similar approach.

2.7.3. Upper and lower bounds for design variables

Upper and lower bound values are defined for design variables to introduce certain end-use and manufacturing constraints. For instance, in depth unconstrained analyses, the lower bound value of l_f, the total width of the flange, is specified as 32 mm to meet the standard requirements set for CFS studs intended for steel framing applications [16]. The lower bound element width for lip elements is set to 5 mm based on the same standard. The lower bound width of web elements is set to 6.35 mm based on the work by Leng et al. [8]. The upper bound values for these elements are determined based on the results obtained. In practice, the lip is usually built perpendicular to the flange, as shown in Fig. 4. However, to allow more freedom to the optimisation process, upper and lower bounds are also set for turn angles. Turn angle of the lip elements (θ_1) is allowed to vary between 45°and 135°. The lower and upper bound values for the turn angles of the web elements (θ_4) are set as 225°and 315°. These bounds are deemed appropriate as very sharp turn angles are difficult to roll form. Furthermore, sharp bends also cause greater loss of ductility in the steel, making its properties more non-uniform across the section.

In the case of depth constrained analyses, the lower bound l_f is taken as 33.5 mm, based on the dimensions of commercially available studs (Fig. 3). Lower bound widths of the lip and web elements are taken as 6.35 mm. The upper bound values are determined after investigating the results obtained. Turn angles θ_1 and θ_4 are fixed at 90°and 270°, respectively, such that the web and the lip are perpendicular to the flange. The turn angles of the internal web elements are determined based on the results obtained.

3. Formulation of the objective function

The choice of suitable optimisation algorithms is made considering the nature of the optimisation problem. Particularly, the formulation of the objective function plays a major role in this regard. The objective function represents a quantitative measure of the "goodness" of a complex system [17]. This optimisation exercise is primarily associated with the enhancement of the axial compression capacity (N_c) of CFS studs. Hence, the determination of the axial compression capacity of complex stud geometries forms the core of the objective function. Conventionally, the Effective Width Method (EWM) has been used in the determination of the capacity of CFS sections. However, the Direct Strength Method (DSM) has emerged as a popular choice in recent years due to the easiness of its application for complex cross sections [18]. Given that optimised CFS cross sections usually tend to take irregular and complex shapes, DSM is considered ideal for the current application.

The Finite Strip Analysis package CUFSM by Li and Schafer [19] allows the user to conduct linear buckling analyses of thin-walled structures such as the studs considered here. CUFSM 3.12 was used in this study to obtain the critical buckling loads of the sections analysed. The axial compression capacities were determined for each of the analysed sections using the DSM. Thus, the fusion of the CUFSM analysis and the DSM calculation formulated the core of the objective function. Steps involved in the calculation of each of the critical buckling loads (N_{cl}, N_{cd}, N_{ce}) using the DSM are presented next.

The nominal member capacity in compression for flexural, torsional or flexural-torsional buckling (N_{ce}), is given by,

$$N_{ce} = \begin{cases} \left(0.658^{{\lambda_c}^2}\right) N_y & \lambda_c \leq 1.5 \\ \left(0.877/{\lambda_c}^2\right) N_y & \lambda_c > 1.5 \end{cases} \tag{1}$$

where, λ_c is the non-dimensional slenderness for determining N_{ce}, given by,

$$\lambda_c = \sqrt{\frac{N_y}{N_{oc}}} \tag{2}$$

where, N_{oc} is the least of the elastic compression member buckling load in flexural, torsional and flexural-torsional buckling, given by,

$$N_{oc} = A f_{oc} \tag{3}$$

where, f_{oc} is the least of the elastic compression member buckling stress in flexural, torsional and flexural-torsional buckling. N_y is the nominal yield capacity of the member in compression, given by,

$$N_y = A f_y \tag{4}$$

N_{cl} is the nominal member capacity in compression for local buckling, given by,

$$N_{cl} = \begin{cases} N_{ce} & \lambda_1 \leq 0.776 \\ \left[1 - 0.15\left(\frac{N_{ol}}{N_{ce}}\right)^{0.4}\right]\left(\frac{N_{ol}}{N_{ce}}\right)^{0.4} N_{ce} & \lambda_1 > 0.776 \end{cases} \tag{5}$$

λ_1 is the non-dimensional slenderness used to determine N_{cl}, given by,

$$\lambda_1 = \sqrt{\frac{N_{ce}}{N_{ol}}} \tag{6}$$

where,

$$N_{ol} = Af_{ol} \tag{7}$$

where, f_{ol} is the critical local buckling stress.N_{cd} is the nominal member capacity in compression for distortional buckling, given by,

$$N_{cd} = \begin{cases} N_y & \lambda_d \leq 0.561 \\ \left[1 - 0.25\left(\frac{N_{od}}{N_y}\right)^{0.6}\right]\left(\frac{N_{od}}{N_y}\right)^{0.6} N_y & \lambda_d > 0.561 \end{cases} \tag{8}$$

λ_d is the non-dimensional slenderness used to determine N_{cd}, given by,

$$\lambda_d = \sqrt{\frac{N_y}{N_{od}}} \tag{9}$$

where,

$$N_{od} = Af_{od} \tag{10}$$

where, f_{od} is the critical distorsional buckling stress. The nominal member capacity of a compression member (N_c) is the minimum of N_{ce}, N_{cl} or N_{cd}. This is expressed as,

$$N_c = min(N_{cl}, N_{cd}, N_{ce})$$

The critical buckling stresses f_{oc}, f_{ol} and f_{od} were determined from the buckling analyses conducted using CUFSM. They were then used int the DSM equations given above to determine the axial compression capacity N_c.

While the objective of this exercise is to identify stud geometries with the greatest axial compression capacities, optimisation problems are usually defined as minimisation problems. Hence, the objective function is given by,

$$min[-N_c(X)]$$

4. Optimisation algorithms

The optimisation algorithms commonly used in similar minimisation problems can be broadly categorised into two. Gradient-based methods calculate the derivatives of the objective function with respect to design variables to determine a solution to the minimisation problem. They are known to be sensitive to the initial guess but are efficient in determining a local minimum. Such algorithms are ideal in cases where the objective function is a continuous one, thus enabling the determination of its derivatives smoothly [8].

Stochastic search methods, on the other hand, utilise random variables to determine the design variables and evaluate the objective function. Due to this, their sensitivity to the initial guess is often found to be lower than that of gradient-based methods, and the likelihood of determining the global minimum is higher. However, they may require a large number of iterations to comprehensively search the design space and thus tend to be slower. Simulated annealing (SA) and Genetic algorithm (GA) are two stochastic search algorithms which have been frequently used in the optimisation of CFS sections previously [3, 6, 8].

The DSM is a function of a variety of variables that can ultimately provide the axial compression capacity of a CFS stud. However, given the discrete nature of the function, gradient-based search algorithms usually struggle to yield desired optimisation results. They show high sensitivity to the initial guess and often return a local minimum. For this reason, the use of stochastic search algorithms is considered ideal for this study. Both SA and GA are used to evaluate the same problems, and the results are compared in the following sections. The analyses are conducted using the Global Optimisation Toolbox of MATLAB R2018a [20].

4.1. Simulated annealing

Annealing is a heat treatment method used in metallurgy where a material is heated beyond its recrystallisation temperature and subsequently cooled, allowing its atoms to rearrange in a controlled manner, decreasing the number of dislocations present in the crystal lattice. This process allows atoms to arrange themselves in the low energy ground state of the lattice, facilitating the alteration of physical and chemical properties such as improved ductility and reduced hardness. Simulated annealing algorithm mimics this process. A parameter termed "Temperature" (T) is specified, with an initial value of T_0, is used to simulate the maximum temperature to which the material is heated. Another parameter termed "cooling" (r) which reduces/tightens with each iteration is also defined to simulate the rate of cooling. Starting with the specified initial design variable values, the axial compression capacity (N_c) is evaluated in each iteration by randomly perturbing the elite design variables. If N_c of the current iteration is superior to that of the preceding one, the elite design is considered to be the one given by the current design. The temperature parameter which started at T_0 reduces at each iteration based on r and governs the frequency of accepting an inferior design. Thus, initially in the search, where T is higher, the probability of accepting an inferior design as the elite design in the current iteration is high. However, due to the progressive reduction in r, which can be governed by a user-defined function, this probability continuously reduces, converging the search towards a minimum. This facilitates the algorithm to better search the design space and increases the chances of locating the global minimum. However, there is no guarantee that the global minimum would be found [3, 21].

The results can be improved by fine-tuning two of the SA options: the initial temperature (T_0) and the rate of cooling (r). A default value of 100 is used for T_0 in this study. This is increased when necessary to increase the chances of determining the global minimum, especially when the number of variables involved is high. In addition to this, the rate of cooling can be altered by changing the function used to update T as the algorithm progresses. By default, the temperature in each iteration is calculated as $T_0 \times 0.95^k$, where k is the iteration number. At times, especially in cases involving higher number of variables, the rate of cooling (r) needs to be reduced to increase the probability of accepting inferior designs as the elite design. Admittedly, this reduces the speed of convergence, but allows the algorithm to search the problem space more comprehensively, thus increasing the chances of determining the global minimum [20]. In this study, the temperature is calculated as $T_o/\ln(k)$ when analysing 8 roller sections which arguably include more variables in their formulation. Fig. 5(a) shows the convergence observed for the 150 mm section without any out-of-plane restraints ($k_y = 0$) under the depth unconstrained analyses using SA.

4.2. Genetic algorithm

A Genetic algorithm (GA) is an optimisation algorithm that is based on natural selection, the process that governs biological evolution. Unlike SA which operates on a single design, GA operates on a population of designs in each iteration. The objective function is evaluated for each design to identify the fittest designs, i.e. the ones giving the highest (or lowest)

objective function values. Such fittest designs selected from the current population are used to generate designs in the new generation by modifying the genome of individual designs. Selection, crossover and mutation are the three types of rules used in the modification of genomes. Selection function determines how the algorithm selects parents for the next generation. The default selection function in MATLAB, Stochastic uniform ('selectionstochunif'), is used in this study. As the design variable is formulated such that the necessity for linear constraints is eliminated, 'crossoverscattered', the default cross over function recommended in MATLAB for such problems, is used. 'mutationgaussian', the default mutation function specified for unconstrained problems in MATLAB, is also used [20].

The population size ('PopulationSize') is set to 80 for most cases. It is increased up to 120 when necessary. Increasing the population size increases the probability of locating the global minimum, as it allows the algorithm to search the design space more comprehensively. The maximum number of generations ('MaxGenerations') is taken as 15 and increased up to 25 based on the observations made. Fig. 5(b) shows the convergence observed for the 150 mm section without any out-of-plane restraints ($k_y = 0$) under the depth unconstrained analyses using GA.

4.3. Implications on the formulation of the problem

It was found that the approach adopted in formulating the problem had a signifncant impact on the outcome of the analysis. A good example is the use of linear equality constraints to have a node in the middle of the flange, equally dividing the total flange length into two. Firstly, this caused the algorithms to struggle finding suitable candidates, and required a large number of iterations just to find the first suitable candidate. Due to the difficulty in ideitifying a diverse range of candidates, the algorithms then tended to limit the optimisation to initial few candidates found. This impaired the ability of the algorithms to comprehensively probe the design space to identify the candidates providing an outcome closer to the global minimum. The reduction process adopted by defining the length variables as interdependent ones eliminated this problem.

5. Results

5.1. Depth unconstrained analyses

5.1.1. Optimisation without out-of-plane (k_y) restraints

The objective function for the depth constrained analyses was the axial compression capacity (N_c). The structural efficiency (N_c/N_y) is used to compare the efficieny between different sections. N_c/N_y is used for the discussion, rather than N_c, becuase the former gives the opportunity to compare the efficiency between different section depths. Given that the strip lengths are fixed for each section depth considered, N_C is proportionaly to N_c/N_y.

Table 2 contains a summary of the optimisation results for the analyses conducted without any out-of-plane (k_y) restraints. However, as stated earlier, full in-plane restraints were present in all the analyses. The optimised sections for the studs with an original section depth of 64 mm are shown next in Fig. 6. In this figure, the optimised sections are drawn to scale, and thus, their dimensions can be obtained from them. The basic section yields the lowest structural efficiency (N_c/N_y) of 0.25. Increasing the number of rollers up to 8 yields a 17% increase in the axial compression capacity and increases the efficiency up to 0.29 (Table 2). The enhancement in N_c recorded is attributed to the increased section depth to about 70 mm due to optimisation and the resulting increase in the critical global buckling strength (f_{oc}). While the critical local buckling strength (f_{ol}) is also found to increase due to the segmentation of the web, its contribution to the enhancement in N_c is minimal.

The optimised sections for the studs with an original section depth of 76 mm are shown in Fig. 7. As seen in Table 2, the N_c of the basic section increases by approximately 25% with the provision of additional rollers. Consequently, the structural efficiency increases from 0.30 to 0.38. f_{ol}, which only amounts to 245 MPa for the basic section, increases up to 400 MPa due to the segmentation of the web during the optimisation process. f_{oc} also increases from 232 MPa to approximately 260 MPa due to the increased section depth to about 80 mm. Thus, the enhancement in N_c obtained with 6 and 8 rollers is attributed to strengthening against both local and global buckling.

The basic 92 mm section possesses an efficiency of 0.33, and with the provision of 6 or 8 rollers, it increases up to 0.49. f_{ol} increases from 170 MPa to approximately 500 MPa due to segmentation of the web. The overall section depth, which was originally 92 mm, is increased to approximately 100 mm by the algorithm for all the optimised sections (Fig. 8). Consequently, f_{oc} shows a marginal increase from 325 MPa to approximately 350 MPa. These result in a 49% maximum increase in N_c. Similar to the previous case, this strength enhancement is a direct result of both local and global buckling strength enhancements.

It is evident from the results presented in Table 2 that the 150 mm basic section has the greatest potential for improvement out of the four basic sections considered. N_c can be increased by up to 169% with the provision of 8 rollers. A closer analysis of the critical buckling stresses in Table 2 shows that this strength enhancement comes from local, distortional and global buckling enhancements. The basic 150 mm deep section yields an efficiency of 0.26. Interestingly, this is lower than those obtained for 76 and 92 mm basic sections. The prime reason for this is the excessive vulnerability of the 150 mm basic section to local buckling of its highly slender web, as indicated by its very low f_{ol} (65 MPa). However, the basic section is very strong against major-axis global buckling, as indicated by an f_{oc} of 754 MPa. This is a direct result of its greater section depth. When provided with only 4 rollers, the optimisation algorithm achieves a balance between the two, reducing the overall section depth, thereby increasing f_{ol} and reducing f_{oc}, ultimately achieving a greater N_c. However, when the number of rollers is increased, the segmentation of the web alleviates the problem of local web buckling, allowing the section to retain its greater section depth. Consequently, as seen in Fig. 9, the overall section depth increases up to 150 mm with the provision of 8 rollers.

5.1.2. Optimisation with 10 N/mm out-of-plane (k_y) restraints

Optimisation results of the four basic sections, conducted with full in-plane restraints and 10 N/mm out-of-plane restraints, are summarised in Table 3. Analysis of the basic 64 mm section yields a structural efficiency of 0.51. Comparatively, 64 mm basic section without any k_y restraints yielded a structural efficiency of 0.25 only (Table 2). The strength enhancement observed in the present analysis is attributed to the enhancement of the critical global buckling stress (f_{oc}), with the provision of additional restraints, as seen in Table 3. Figs. 10(a) and (b) show that optimisation process identifies the contribution made by the additional 10 N/mm k_y restraints towards global buckling strength enhancement and reduces the overall section depth to enhance the local buckling strength accordingly. Increasing the number of rollers allows the web depth to be increased without compromising the local buckling strength. As such, with increasing number of rollers, the overall section depth is increased to spread the mass further away from the centroidal axis and enhance the global buckling strength. Consequently, with increasing number of rollers, both N_c and structural efficiency improve. Interestingly, the percentage increases in N_c achieved are greater than those achieved previously for the 64 mm sections without any out-of-plane restraints. Thus, the inclusion of these additional sheathing restraints allows the optimisation process to bring in incremental benefits.

Fig. 11 shows the optimised sections with 10 N/mm k_y restraints for the 76 mm basic stud. Similar observations

to those described earlier are made. The 4 roller 76 mm basic stud is found to be very prone to local buckling. Thus, utilising the additional restraints given by the k_y restraints, the 4 roller optimised stud possesses a lower stud depth of approximately 47 mm, as shown in Figs. 11(a) and (b). However, increasing the number of rollers eliminates this deficiency and allows the overall stud depth to be increased. This facilitates the enhancement of f_{oc}. Consequently, incremental strength enhancements are achieved, as shown in Table 3.

Shown in Fig. 12 are the optimised 92 mm sections with 10 N/mm k_y restraints. Similar observations to those made earlier are made. With an f_{ol} of only 170 MPa, the basic 92 mm section is highly vulnerable to local buckling. 4 roller optimised sections, therefore, have shorter webs, as seen in Figs. 12(a) and (b). Provision of 6 to 8 rollers facilitates the enhancement of f_{ol} through segmentation of the web, making greater stud depths structurally feasible. Consequently, overall section depths closer to the original 92 mm are achieved, while enhancing N_c by up to 60% (Table 3).

Fig. 13 shows the optimised sections with 10 N/mm k_y restraints for the 150 mm basic stud. The greatest enhancements in N_c are achieved for these 150 mm sections, as shown in Table 3. The optimisation process reduces the overall section depth from 150 mm to around 70 mm for the 4 roller option, signifying the prominence of local buckling. Greater section depths become feasible when provided with additional rollers. In fact, by providing 8 rollers, the section depth can be retained at around 150 mm, while almost tripling the axial compression capacity (Table 3).

5.1.3. Optimisation with 20 N/mm out-of-plane (k_y) restraints

The following sections present optimisation results for analyses conducted with full in-plane restraints and 20 N/mm out-of-plane restraints. The 64 mm optimised sections are shown in Fig. 14. The axial compression capacity of the basic section can be increased by up to 37%, as shown in Table 4, with the provision of 6 or 8 rollers. Consequently, the structural efficiency goes up to a maximum of 0.75. In contrast, the greatest percentage increases attained in the previous two analyses for the 64 mm sections are 17% and 25% only. Thus, it is reconfirmed that the inclusion of larger sheathing restraints improves the optimisation outcome.

The structural efficiency of the basic 76 mm section with 20 N/mm k_y restraints amounts to 0.51. N_c can be enhanced by up to 47%, as shown in Table 4, by increasing the number of rollers to 6 or 8. Shown next in Fig. 15 are the optimised sections found.

Fig. 16 shows the optimised studs for 92 mm sections with 20 N/mm k_y restraints. Similar trends to those observed earlier prevail. Table 4 shows that the 55 kN N_c of the basic 92 mm section could be enhanced by 68% to 92 kN with the provision of 6 to 8 rollers. The overall section depth under these conditions remains closer to the 92 mm original section depth.

Shown in Fig. 17 are the optimised 150 mm studs with 20 N/mm k_y restraints. They clearly show the effects of additional rollers on the overall depth of the section. As previously observed, the greatest strength enhancements are observed for these sections. The axial compression capacity of the basic 150 mm section can be enhanced by 200% with the provision of 8 rollers. This results in the structural efficiency increasing to 0.79. In fact, this is the greatest structural efficiency recorded in all the analyses.

5.2. Depth constrained analyses

The optimised sections presented earlier do not strictly conform to the standard section depths used in the industry (64, 76, 92 and 150 mm). In fact, they prove that by using the same amount of steel as that used in a standard section, highly optimised non-standard sections can be developed. However, given that the standard section depths are

well established in the industry, it is worthwhile developing sections that conform to these depth requirements while incorporating optimisation to the greatest possible extent.

In the search for optimised sections with standard section depths, analyses are conducted using both SA and GA algorithms. A few modifications are deemed necessary to the original formulations to accommodate the depth constrained analyses. The overall strip width was used as a governing parameter in previous depth unconstrained analyses. In depth constrained analyses, the depth of the section (web depth) is treated as a governing parameter. i.e. depths of all the web elements add up to the governing section depth in each analysis. These section depths are set as 64, 76, 92 and 150 mm for the four sections. The lip length and flange width are only bound by their respective upper and lower bounds. Hence, the total strip length and the cross sectional area of the strip may vary in each iteration of a given analysis. The variation of the cross sectional area makes the use of N_c as the objective function value unsuitable. Thus the original objective function used in depth unconstrained analyses ($min(-N_c(X))$) is normalised as,

$$min\left[-\frac{N_c(X)}{N_y(X)}\right] \tag{11}$$

where, N_y is the yield load of the design section, given by,

$$N_y = A_g \times f_y \tag{12}$$

where, A_g is the cross sectional area of the design section, and f_y is the yield strength of steel.

The use of this normalised function in its current form as the objective function causes the algorithms to often choose sections with greater cross sectional areas as optimum sections. However, it is known that a balance between efficiency and economy is always preferred by the industry. Thus, a penalty clause (A_g/A_{Basic}) is introduced together with a penalty factor (α) to the objective function to favour lower cross sectional area solutions as,

$$min\left[-\frac{N_c(X)}{N_y(X)} + \frac{A_g}{A_{Basic}} \times \alpha\right] \tag{13}$$

The cross sectional areas of the basic sections (A_{Basic}) were presented earlier in Table 1. A penalty factor (α) of 0.2 was used for all the analyses. Thus, the algorithms yield structurally optimised minimum weight solutions which conform to the standard depths used in the industry. Gilbert et al. [7] followed a similar procedure to determine optimum sections with minimum cross sectional area that yield the highest capacities.

Full in-plane translational restraints are provided to simulate the in-plane bracing effect provided to LSF wall studs by the sheathing. The effects of out-of-plane restraints on the current optimisation process are found to be minimal as the section depth is constrained at fixed values. Therefore, no out-of-plane (k_y) restraints are included in the analyses, and the results are compared against those presented in Table 2. The number of rollers is kept constant at 8 as this proved to bring the greatest enhancements in all four sections analysed. The following section presents these optimised stud shapes that conform to each of the section depths considered. Fig. 18 shows each of these optimised stud shapes. A summary of the details of these optimised sections is presented in Table 5.

5.2.1. 64 mm sections

Fig. 18(a) shows the optimised stud found by the optimisation algorithms which conforms to the 64 mm section depth requirement. Due to its already lower section depth, segmentation of the web does not increase the axial compression capacity of 64 mm sections significantly. Thus, the incremental benefits of providing additional rollers are minimal.

The algorithms, therefore, eliminate the web-stiffener by keeping the web straight. The marginal strength enhancements recorded during the previous depth unrestricted optimisation process, as seen in Table 2, are mostly due to the increase in the section depth (Fig. 6) and the resulting increase in the critical global buckling strength (f_{oc}). If the necessity to keep the overall section depth at 64 mm is reintroduced, with a structural efficiency of 0.25, the basic 64 mm section geometry shown in Fig. 4(a) remains to be the best available section.

5.2.2. 76 mm sections

Shown in Fig. 18(b) is the depth conforming optimised shape proposed for 76 mm deep sections. With full in-plane restraints and no out-of-plane restraints, this stud is capable of reaching a structural efficiency of 0.33. This is greater than that of the 76 mm basic stud (0.30). However, it is lower than the greatest achievable efficiency of 0.38 (Table 2) due to the restriction of the overall section depth to 76 mm. The lip length and the flange width are brought to their minimum values. The depth of the web stiffener amounts to approximately 5 mm. In contrast, the web-stiffened stud used in all the tests in this study had a 10 mm deep stiffener. Thus, the optimisation process has redistributed this additional mass to the vertical web components as it aids to spread the mass further away from the centroidal axis in the most optimum way, increasing f_{oc} and N_c.

5.2.3. 92 mm sections

The section shown in Fig. 18(c) conforms to the 92 mm depth requirement and is an optimised alternative to the 92 mm basic stud (Fig. 4(c)). This optimised section has a structural efficiency of 0.45, whereas the basic section had an efficiency of only 0.33 (Table 2). In contrast, the 90 mm deep web-stiffened stud possessed a structural efficiency of 0.43. Hence, the proposed stud is marginally structurally superior to the web-stiffened stud. Similar to the earlier case, the lip length and the flange width are kept at their minimum values. The depth of the web stiffener in this optimised stud also amounts to approximately 5 mm. Overall, this 92 mm deep optimised stud is identified as a structurally superior alternative with minimal incremental fabrication costs to the basic stud used by the industry at present.

To ensure that out-of-plane restraints have no significant influence over the depth constrained optimisation analyses, the depth constrained 92 mm sections were also analysed with 10 and 20 N/mm k_y restraints. Fig. 19 shows that the optimised shapes obtained for the three cases (0, 10 and 20 N/mm) are very similar. To compare the performance of these three sections on a neutral level, they are re-analysed using the finite strip method without any k_y restraints (full in-plane restraints were provided in all three sections) and evaluated using the DSM. A summary of the results are presented in Table 6. It shows that when the effects of k_y restraints are removed from the analysis, all three sections yield a structural efficiency of 0.45. The limitations imposed on the design space by the fixed web depth, flat flanges and penalty on the area are identified as the reasons behind this outcome.

5.2.4. 150 mm sections

Shown in Fig. 18(d) is the optimised section geometry which conforms to the 150 mm section depth requirement. In contrast to the 0.26 structural efficiency of the 150 mm basic stud (Table 2), this optimised 150 mm stud possesses a significantly greater structural efficiency of 0.71. While the flange width is kept at its minimum value of 33.5 mm, the lip length is increased to approximately 11 mm by the optimisation process. A stiffener depth of approximately 14 mm is set by the optimisation algorithms.

6. Discussion of shape optimisation studies

6.1. Comparison between SA and GA

In general, both SA and GA often yield similar results for a given case. With 6 and 8 roller sections, the GA, at times, provides sections with marginally superior performance than those provided by SA. Both these stochastic algorithms yield approximate solutions to the optimisation problem. There is no guarantee that the global minimum is found. However, the probability of determining a close approximate solution to the global minimum can be increased by fine-tuning the algorithms, as done in this study. Thus, differences in the turn angles are noticeable. However, more primary overall dimensional properties such as the lip and flange widths, and the web depth are often similar for a given number of rollers.

6.2. Trends in the depth unconstrained optimisation analyses

The basic sections with 4 rollers yield the lowest axial compression capacities. In general, increasing the number of rollers beyond 4 increases the axial compression capacity (N_c). Investigation of the three critical buckling stresses reveals that a root cause for the enhancement of N_c with the provision of more rollers is the suppression of the local buckling failure of the web. Enhancement of the critical local buckling stress (f_{ol}) is a result of the segmentation of the otherwise slender web. Introduction of additional rollers converts the web into an assembly of shorter, stiffer plate elements and reduces the overall slenderness of the section.

The strengthening of the web through segmentation allows the web depth to be increased without compromising the local buckling performance. An increase in the web depth also increases the overall depth of the section. Therefore, with increasing number of rollers, sections become deeper, and have their masses spread further away from their major axis. Furthermore, with increasing number of rollers, the significance of having a lip also diminishes, and this mass is added to the web to increase the overall depth of the section. This can clearly be seen in the optimised 150 mm sections. These alterations enhance the radius of gyration (r_{xx}) and the second moment of area (I_{xx}) of the section about its major axis. Thus, the optimisation process reduces the member slenderness and enhances the resistance against global buckling about the major axis. Consequently, with increasing number of rollers, the critical global buckling stress (f_{oc}) also increases, as evident from Tables 2 to 4. It is reiterated here that buckling about the minor axis is eliminated through the use of full in-plane lateral restraints. Thus, it becomes acceptable for the optimised studs to possess a lower radius of gyration (r_{yy}) and second moment of area (I_{yy}) about the minor axis. Consequently, in most cases, the optimisation process determines that the flange width can be reduced to its lower bound value of 32 mm. The additional mass contained within the flange is redistributed within the web, further increasing the overall depth of the section.

Another critical observation is that the potential for strength enhancement increases significantly with increasing section sizes. 64 mm sections record the lowest levels of percentage enhancement in N_c. 150 mm sections, on the other hand, have the potential for significant gains in the order of 200%. The reason behind this is that in their basic form, larger sections are structurally inferior to smaller ones due to extremely poor local buckling performance. For instance, the 150 mm basic section (Fig. 4(d)), despite having a greater cross sectional area, has a lower structural efficiency compared to the 64 mm basic section (Fig. 4(a)), as seen in the tabulated results. However, larger sections offer more freedom for the optimisation process and have greater potential for strengthening against local and global buckling. Smaller sections such as the 64 mm one, on the other hand, are restricted by their lower steel strip widths and are unable to significantly improve the critical global buckling strength by spreading the mass away from the centroidal axis. Their critical local buckling strengths are naturally high due to shorter web depths. These restrict the room for further optimisation.

With increasing number of rollers, the incremental benefits of additional rollers diminish, and the structural efficiency (N_c/N_y) reaches a maximum. In the case of smaller sections such as the 64 mm one, this is reached very early, as the results for both 6 and 8 roller options are very similar. Thus, the provision of 10 or more rollers is deemed impractical and unnecessary for such sections. The situation is similar for 76 mm and 92 mm sections as well. 150 mm sections, however, indicate a clear distinction between the optimisation results for 6 and 8 roller options. This is again an effect of the greater strip length of the 150 mm section which allows the enhancement of the section depth with increasing number of rollers, as seen in Figs. 9, 13 and 17. Hence, optimisation of the 150 mm section was also conducted with 10 rollers. However, it revealed that the incremental benefits with 10 rollers are minimal compared to 8 rollers.

Depth unconstrained optimisation analyses conducted incorporating 10 and 20 N/mm k_y restraints revealed that the inclusion of these additional restraints allowed the optimisation process to be enhanced further. Particularly, these additional global restraints facilitated the shortening of the section depth of 4-roller sections, thereby improving their local buckling strength. In the case of 6 and 8-roller sections, they facilitated the section depths to be increased close to their original values.

6.3. Summary of depth constrained optimisation analyses

As seen in Table 5, the depth constrained 76 and 92 mm optimised sections require 2% more steel compared to their basic section. The 150 mm section requires 9% more steel than its basic section. Hence, the incremental material cost is only marginal. The optimised studs only require the deployment of additional rollers. Overall, it is evident that significant structural benefits can be attained, especially with deeper sections, with the introduction of web-stiffeners, while retaining their original section depths. It is also confirmed that the inclusion of k_y restraints does not significantly influence the depth constrained analyses as Fig. 19 shows that 92 mm sections, when analysed with varying k_y restraints, yield similar optimised shapes.

7. Implications on sections of different thicknesses

This study has exclusively optimised the 1.15 mm thick cold-formed steel LSF wall studs currently used in the industry. CFS sections of different thickness (0.55 mm, 0.75 mm and 0.95 mm) are also used as LSF wall studs. These sections can also be optimised in a similar manner using the same methodology. However, the optimised stud shapes proposed for 1.15 mm studs should not be taken as the same for sections of different thickness. Due to the lower material thickness and the resulting higher plate slenderness, 0.55, 0.75 and 0.95 mm sections would likely require the deployment of more rollers. It is expected that the strength enhancements obtained with optimisation would be greater in these thinner sections because their basic geometries are more prone to local buckling compared to the thicker 1.15 mm sections. Hence, optimisation of these sections is recommended for future work.

8. Comparison against the web-stiffened stud

Fig. 20 shows a direct comparison of the 92 mm basic stud currently used in the industry, the 90 mm web-stiffened stud used in previous studies [14] and the newly found 92 mm depth constrained optimised stud. A comparison of their capacities and structural efficiencies, conducted using both FSM and FE analyses, are presented in the following section.

8.1. Comparison of FSM analysis results

The web-stiffened stud used in [14] was folded from a 191 mm wide 1.15 mm G500 steel strip (f_y = 610 MPa)(Table 1). Using the finite strip method and the DSM guidelines, the capacity of a 3 m long web-stiffened stud with full in-plane translational restraints and no out-of-plane restraints is estimated to be 55.8 kN. Consequently, structural efficiency (N_c/N_y) of the web-stiffened stud amounts to approximately 0.42.

This 90 mm deep web-stiffened stud is comparable with the 92 mm basic lipped channel stud (Fig. 4(c)) and the depth constrained 92 mm optimised stud (Fig. 20(c)). The axial compression capacity (N_c) and the structural efficiency of the basic lipped channel section, calculated using the same method, amounted to only 39.9 kN and 0.33, respectively. The depth constrained 92 mm optimised section yielded an efficiency of 0.45, along with an N_c of 55.6 kN. Thus, the depth constrained optimised stud appeared as the most superior candidate. Table 7 shows a summary of the results. The cross sectional areas of each of these sections derived from CUFSM and those calculated based on the centre line dimension for the FE analyses discussed next are included in this table, separately. Likely due to corner rounding effects, the cross sectional areas given by CUFSM were often slightly smaller than those calculated from the centre line dimensions of Abaqus FE models. The respective A_g values were used when calculating the structural efficiencies from finite strip and finite element analyses in Table 7.

8.2. Comparison of FE analysis results

The three sections shown in Fig. 20 were also analysed using the FE software Abaqus CAE. Single-stud unsheathed and single-stud sheathed FE modelling techniques were used to model the three studs. A summary of the results and the cross sectional areas of the three studs calculated based on the centre-line dimensions of the FE models of the studs are presented in Table 7. The results of the single-stud unsheathed FE analyses revealed that the lipped channel section yielded the lowest N_c (43.5 kN) and the lowest structural efficiency (0.34). The 90 mm web-stiffened stud and the 92 mm depth constrained optimised stud reached axial compression capacities of 66.7 and 59.5 kN, respectively. It is noteworthy that the optimised stud yielded a lower N_c than the web-stiffened stud because the cross sectional area of the former is less than that of the latter. However, the structural efficiency of the optimised stud (0.49) is greater than that of the web-stiffened stud (0.47). Hence, the single-stud unsheathed FE models also revealed the 92 mm depth constrained stud to be the most superior stud.

The capacities and efficiencies of the three studs were finally analysed using single-stud sheathed FE models. Unlike in single-stud unsheathed FE models, the sheathing was also modelled explicitly along with suitable mechanical properties. Double plasterboard sheathing was selected as the sheathing configuration for the present analysis. The double plasterboard sheathed 92 mm lipped channel stud reached a failure load of 70.9 kN and a structural efficiency of 0.56, as shown in Table 7. In contrast, the 90 mm web-stiffened stud failed at 101.7 kN along with an efficiency of 0.72. The 92 mm depth constrained optimised stud yielded an N_c of 87.8 kN and and efficiency of 0.73. Thus, the sheathed FE models also confirmed that the 92 mm depth constrained optimised stud is the most superior section. Details of FE models are given in [14, 22].

The FSM analyses shown earlier yielded 0.33, 0.42 and 0.45 as the structural efficiencies for the 92 mm lipped channel, 90 mm web-stiffened stud and the 92 mm depth constrained optimised stud, respectively. In contrast, the efficiency values of the unsheathed FE analyses are marginally greater. This is plausible given that the DSM estimates are conservative compared to finite element calculations. Interestingly, although the sheathed FE models follow the same trend, confirming the optimised stud to be the superior candidate, they yield significantly greater capacities and efficiencies compared to

FSM analyses and unsheathed FE analyses. This is due to the incorporation of the out-of-plane sheathing stiffness (k_y) by the sheathed FE model. Overall, it reveals that when sheathed with double plasterboards, the 92 mm optimised stud can be highly structurally efficient, yielding material and cost savings to the user.

Despite their superior structural efficiencies, the unconstrained optimised studs are unlikely to be acceptable to the industry due to their non-standard geometry. The web-stiffened stud, despite having proven to be very efficient through testing in [14], appears to be marginally inferior to the optimised studs. Thus, the constrained optimised 92 mm section is identified as the ideal candidate which satisfies both superior structural efficiency and standard section geometry requirements. In fact, all the depth constrained optimised studs shown in Fig. 18 are recommended as structurally superior practically feasible alternatives to the basic studs used in the industry at present.

9. Conclusion

This paper has presented the results of an optimisation study conducted using Simulated annealing (SA) and Genetic algorithm (GA) optimisation algorithms to determine optimised light gauge steel-framed (LSF) wall studs with greater structural efficiency. Particularly, the restraints provided to LSF wall studs by the sheathing were idealised and included in the optimisation process. Optimisation analyses were conducted for 1.15 mm thick LSF wall studs of four different standard sizes used in the industry. Optimised sections with significant strength and efficiency enhancements were found. The sources of strength enhancement and the influence of sheathing restraints were investigated. Comparisons were made between the optimised stud sections identified from this study and the web-stiffened stud used in a previous experimental study [14]. Structurally superior alternatives to the basic LSF wall studs presently used in the industry, with minimal incremental fabrication costs, were proposed. In addition to these, this study also showed that advanced FE modelling methods could be successfully used to verify the capacity enhancements provided by the optimised stud sections. The optimised stud shapes are in general agreement with the web-stiffened stud geometries in current use, but with variations in element lengths and turn angles, which can potentailly be incorporated in production with minimal incremental costs.

Acknowledgement

The authors wish to thank QUT for providing a PhD scholarship and research facilities to the first author. They also wish to thank Dr Poologanathan Keerthan for his support to the first author in the initial stages of his PhD study.

References

[1] P. A. Seaburg, C. G. Salmon, Minimum weight design of light gage steel members, Journal of the Structural Division 97 (1) (1971) 203–222.

[2] Y. Tian, T. Lu, Minimum weight of cold-formed steel sections under compression, Thin-Walled Structures 42 (4) (2004) 515–532.

[3] J. Leng, J. K. Guest, B. W. Schafer, Shape optimization of cold-formed steel columns, Thin-walled structures 49 (12) (2011) 1492–1503.

[4] H. Liu, T. Igusa, B. Schafer, Knowledge-based global optimization of cold-formed steel columns, Thin-Walled Structures 42 (6) (2004) 785–801.

[5] J. Lee, S.-M. Kim, H. S. Park, Optimum design of cold-formed steel columns by using micro genetic algorithms, Thin-Walled Structures 44 (9) (2006) 952–960.

[6] B. P. Gilbert, L. H. Teh, H. Guan, Self-shape optimisation principles: Optimisation of section capacity for thin-walled profiles, Thin-Walled Structures 60 (2012) 194–204.

[7] B. P. Gilbert, T. J.-M. Savoyat, L. H. Teh, Self-shape optimisation application: Optimisation of cold-formed steel columns, Thin-walled structures 60 (2012) 173–184.

[8] J. Leng, Z. Li, J. K. Guest, B. W. Schafer, Shape optimization of cold-formed steel columns with fabrication and geometric end-use constraints, Thin-Walled Structures 85 (2014) 271–290.

[9] D. Phan, S. M. Mojtabaei, I. Hajirasouliha, J. Ye, J. Lim, Coupled element and structural level optimisation framework for cold-formed steel frames, Journal of Constructional Steel Research (2019) 105867doi:10.1016/j.jcsr.2019.105867.

[10] J. Ye, I. Hajirasouliha, J. Becque, K. Pilakoutas, Development of more efficient cold-formed steel channel sections in bending, Thin-Walled Structures 101 (2016) 1 – 13. doi:https://doi.org/10.1016/j.tws.2015.12.021.
URL http://www.sciencedirect.com/science/article/pii/S0263823115301841

[11] J. Ye, I. Hajirasouliha, J. Becque, A. Eslami, Optimum design of cold-formed steel beams using particle swarm optimisation method, Journal of Constructional Steel Research 122 (2016) 80 – 93. doi:https://doi.org/10.1016/j.jcsr.2016.02.014.
URL http://www.sciencedirect.com/science/article/pii/S0143974X16300384

[12] J. Ye, S. M. Mojtabaei, I. Hajirasouliha, Local-flexural interactive buckling of standard and optimised cold-formed steel columns, Journal of Constructional Steel Research 144 (2018) 106 – 118. doi:https://doi.org/10.1016/j.jcsr.2018.01.012.
URL http://www.sciencedirect.com/science/article/pii/S0143974X17309628

[13] J. Ye, J. Becque, I. Hajirasouliha, S. M. Mojtabaei, J. B. Lim, Development of optimum cold-formed steel sections for maximum energy dissipation in uniaxial bending, Engineering Structures 161 (2018) 55 – 67. doi:https://doi.org/10.1016/j.engstruct.2018.01.070.
URL http://www.sciencedirect.com/science/article/pii/S0141029617311355

[14] Y. Dias, M. Mahendran, K. Poologanathan, Axial compression strength of gypsum plasterboard and steel sheathed web-stiffened stud walls, Thin-Walled Structures 134 (2019) 203–219.

[15] Rondo Building Systems, Steel framing installation guide, Tech. rep. (2013).

[16] ASTM, Astm c 645 - 04a standard specification for nonstructural steel framing members, Tech. rep., Washington, DC (2004).

[17] S. Kirkpatrick, C. D. Gelatt, M. P. Vecchi, Optimization by simulated annealing, science 220 (4598) (1983) 671–680.

[18] B. W. Schafer, The direct strength method of cold-formed steel member design, Journal of constructional steel research 64 (7-8) (2008) 766–778.

[19] Z. Li, B. W. Schafer, Buckling analysis of cold-formed steel members with general boundary conditions using cufsm conventional and constrained finite strip methods, in: Proceedings of the 20$^{\text{th}}$ International speciality conference on cold-formed steel structures, St. Louis, Missouri, USA, 2010, pp. 17–31.

[20] I. The MathWorks, MATLAB and Statistics Toolbox Release 2018a, R Foundation for Statistical Computing, Natick, Massachusetts, United States (2018).
URL `https://www.mathworks.com/products/global-optimization.html`

[21] P. J. van Laarhoven, E. H. Aarts, Simulated annealing, in: Simulated annealing: Theory and applications, Springer, 1987, pp. 7–15.

[22] Y. Dias, P. Keerthan, M. Mahendran, Predicting the fire performance of lsf walls made of web stiffened channel sections, Engineering Structures 168 (2018) 320–332.

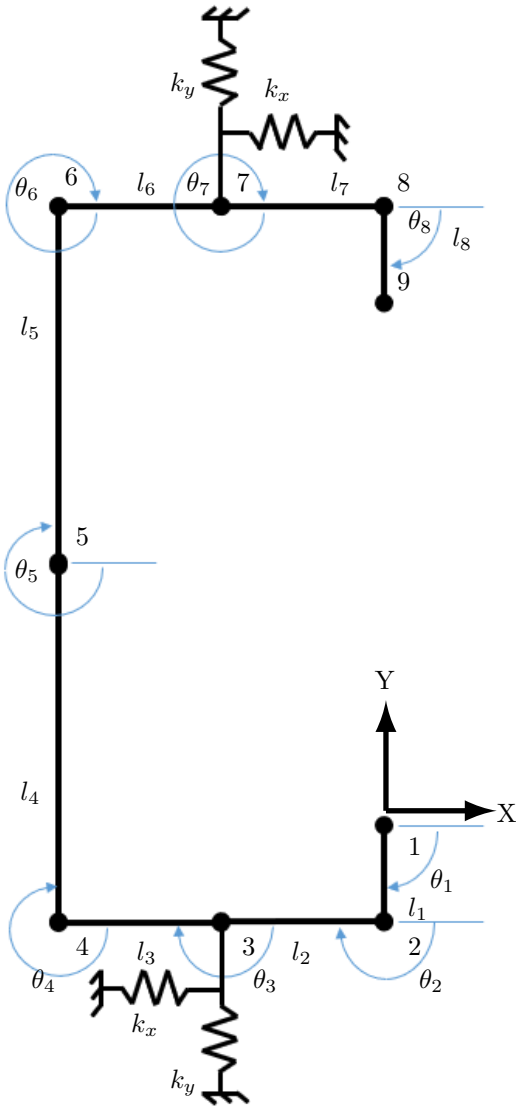

Fig. 1. Definition of design variables

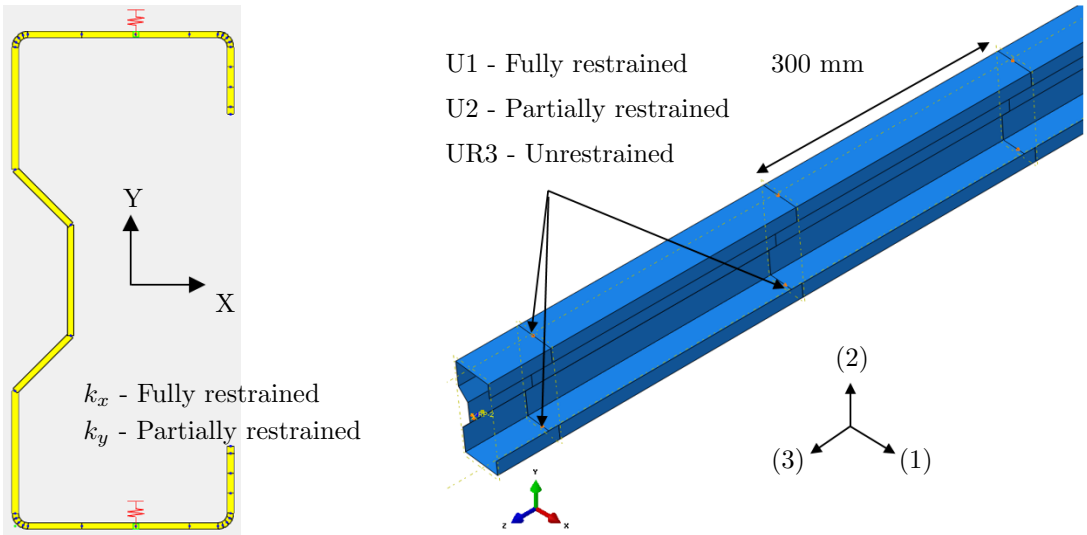

(a) CUFSM **(b)** Abaqus

Fig. 2. Simulation of Lateral Restraints in Numerical Models

Fig. 3. Basic LSF wall stud geometries [15]

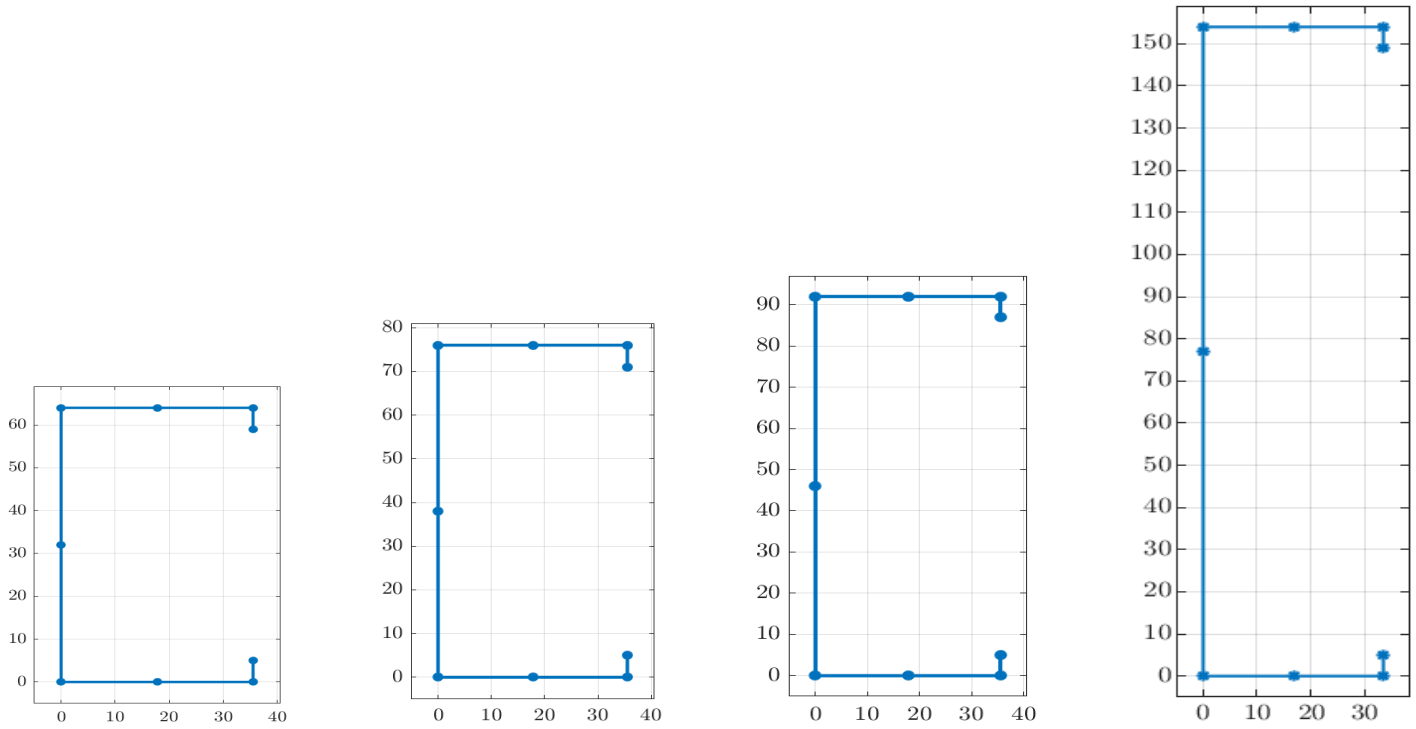

(a) 64 mm stud **(b)** 76 mm stud **(c)** 92 mm stud **(d)** 150 mm stud

Fig. 4. Basic studs

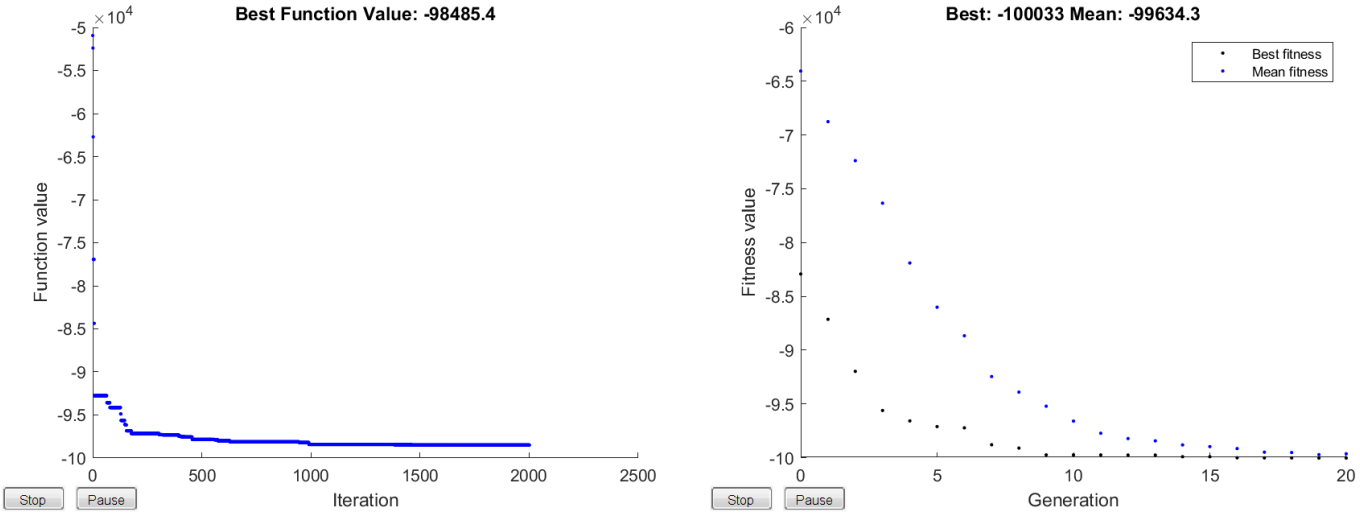

(a) Convergence in SA **(b)** Convergence in GA

Fig. 5. Convergence in SA and GA for depth unconstrained, 150 mm section with $k_y = 0$

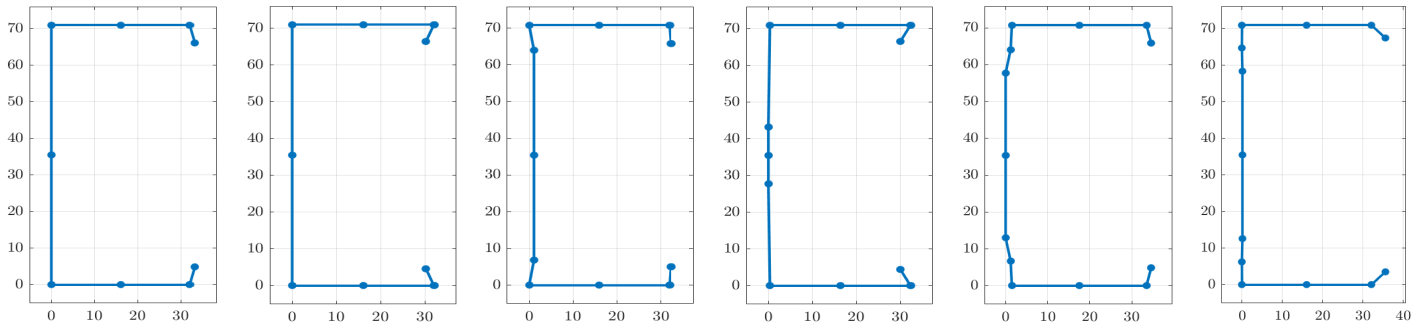

(a) 4-SA **(b)** 4-GA **(c)** 6-SA **(d)** 6-GA **(e)** 8-SA **(f)** 8-GA

Fig. 6. 64 mm stud optimisation results, $k_y = 0$

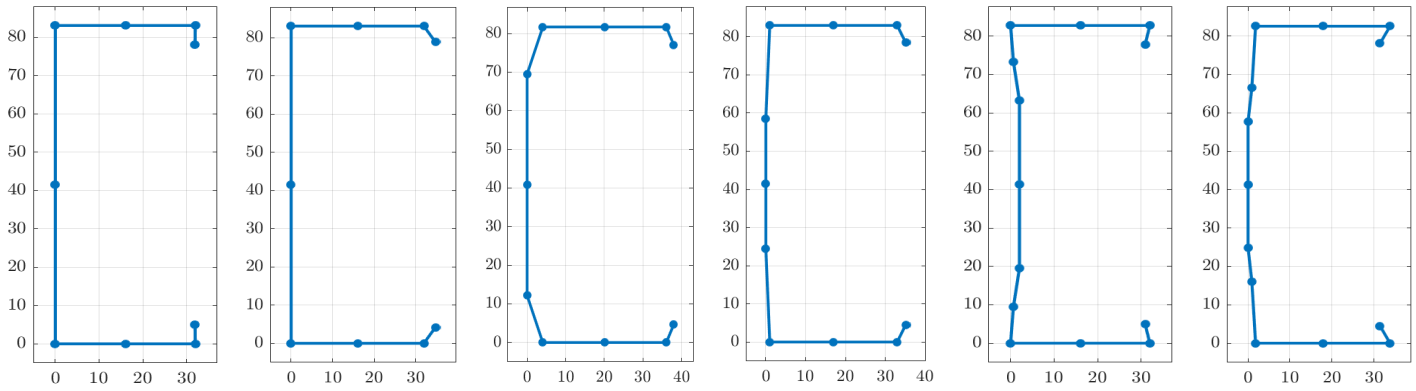

(a) 4-SA **(b)** 4-GA **(c)** 6-SA **(d)** 6-GA **(e)** 8-SA **(f)** 8-GA

Fig. 7. 76 mm stud optimisation results, $k_y = 0$

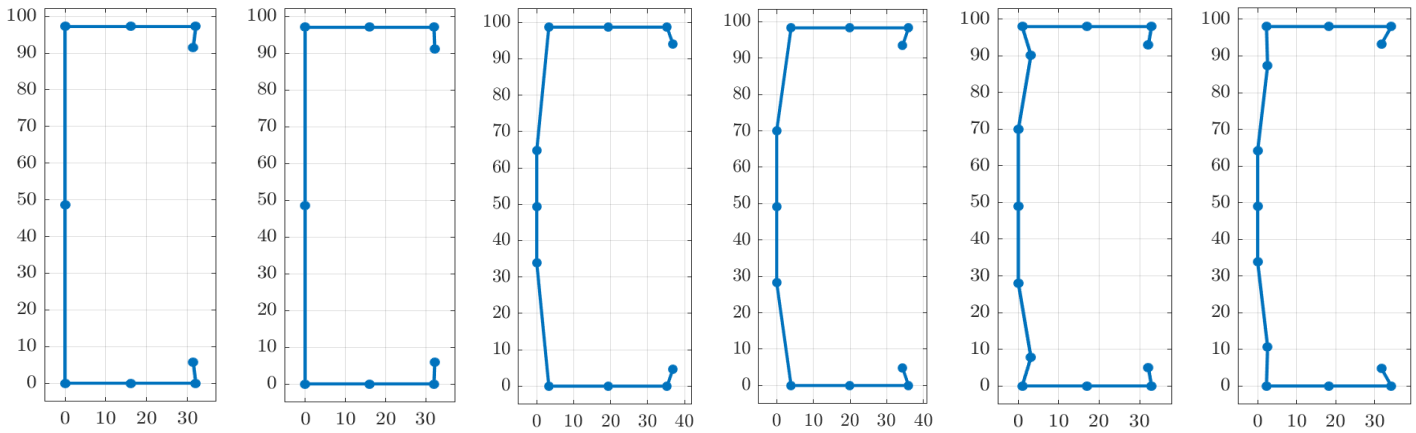

(a) 4-SA **(b)** 4-GA **(c)** 6-SA **(d)** 6-GA **(e)** 8-SA **(f)** 8-GA

Fig. 8. 92 mm stud optimisation results, $k_y = 0$

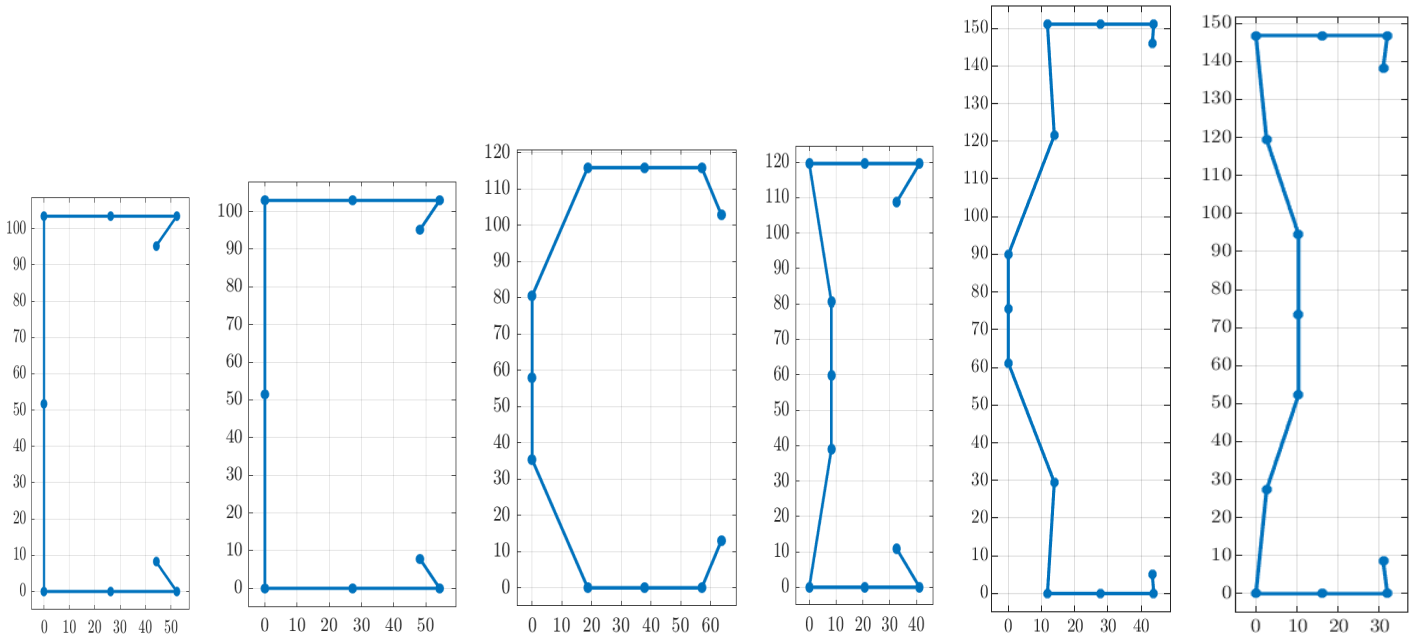

(a) 4-SA **(b)** 4-GA **(c)** 6-SA **(d)** 6-GA **(e)** 8-SA **(f)** 8-GA

Fig. 9. 150 mm stud optimisation results, $k_y = 0$

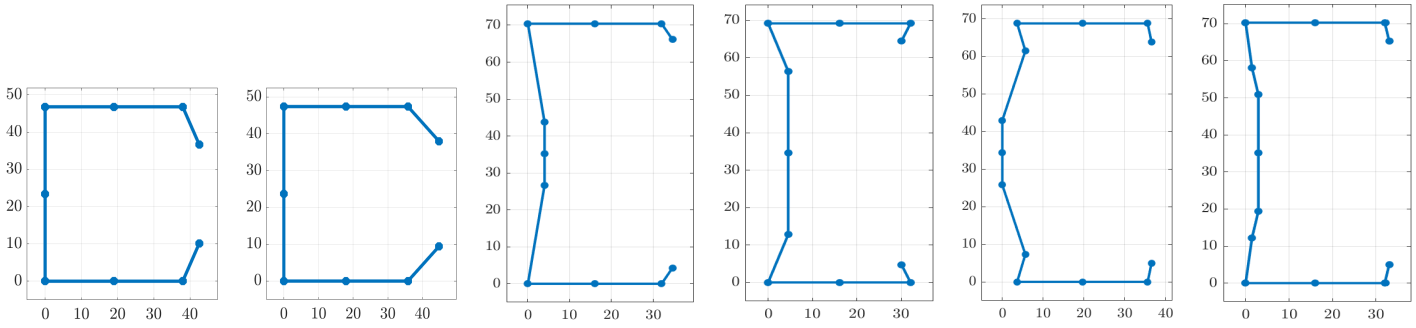

(a) 4-SA **(b)** 4-GA **(c)** 6-SA **(d)** 6-GA **(e)** 8-SA **(f)** 8-GA

Fig. 10. 64 mm stud optimisation results, $k_y = 10$ N/mm

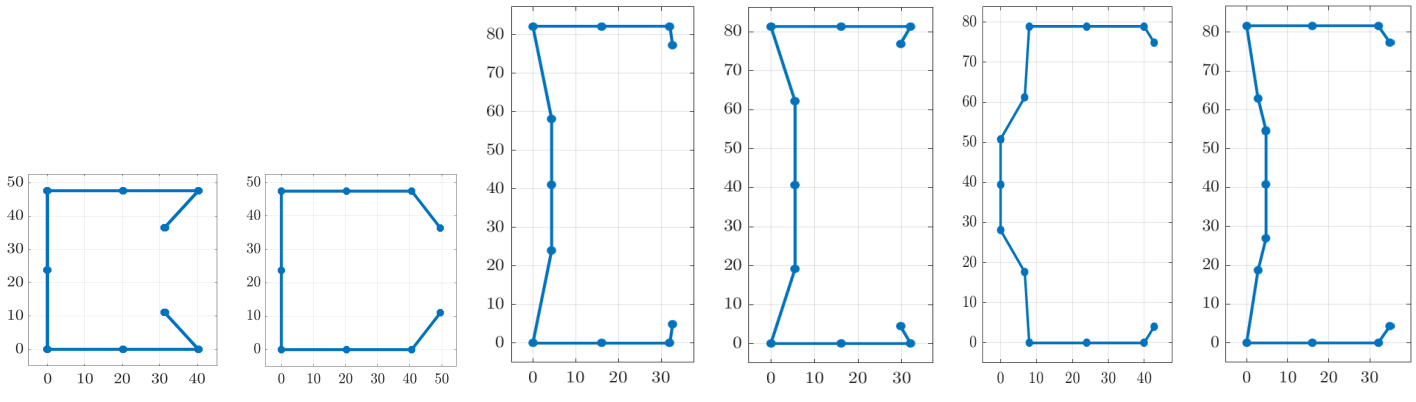

(a) 4-SA **(b)** 4-GA **(c)** 6-SA **(d)** 6-GA **(e)** 8-SA **(f)** 8-GA

Fig. 11. 76 mm stud optimisation results, $k_y = 10$ N/mm

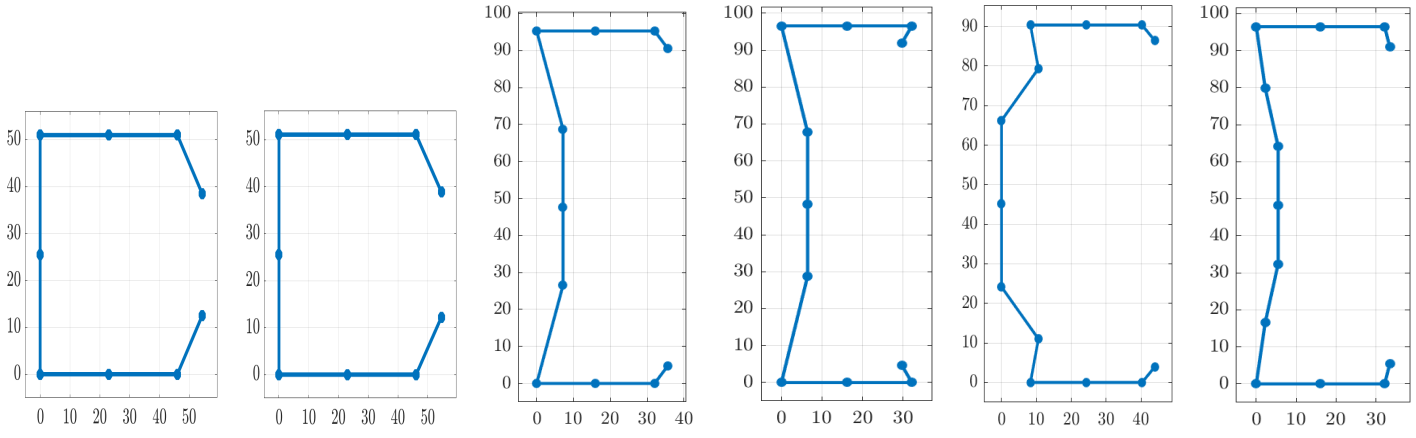

(a) 4-SA **(b)** 4-GA **(c)** 6-SA **(d)** 6-GA **(e)** 8-SA **(f)** 8-GA

Fig. 12. 92 mm stud optimisation results, $k_y = 10$ N/mm

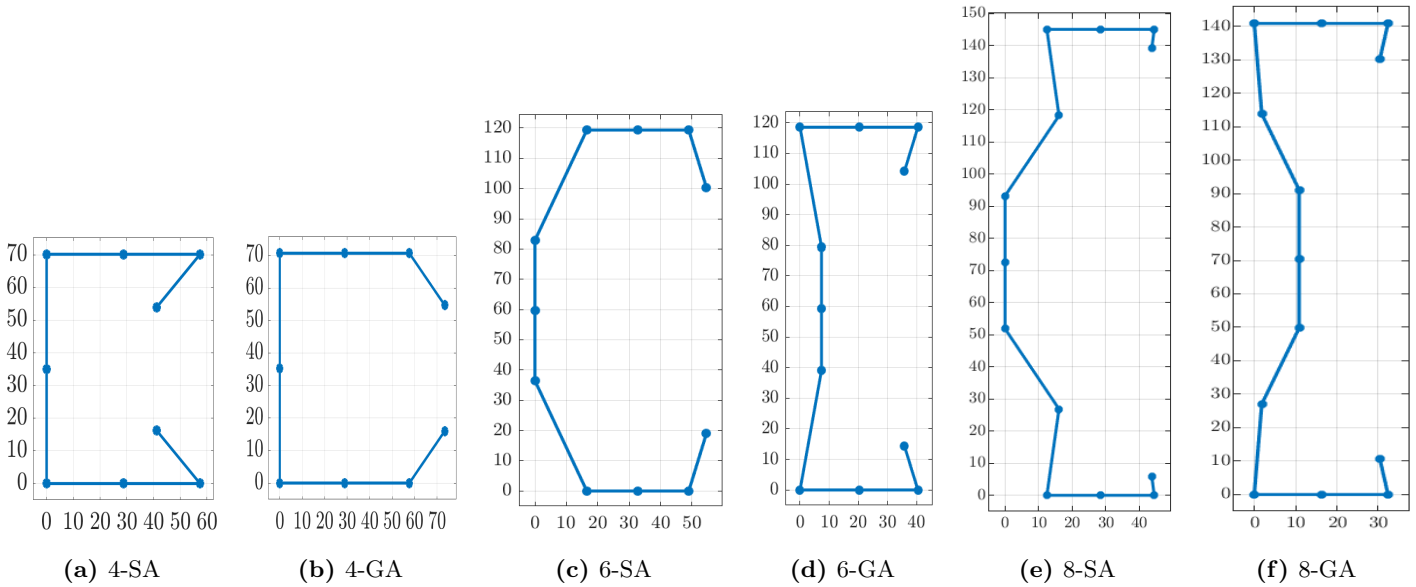

(a) 4-SA **(b)** 4-GA **(c)** 6-SA **(d)** 6-GA **(e)** 8-SA **(f)** 8-GA

Fig. 13. 150 mm stud optimisation results, $k_y = 10$ N/mm

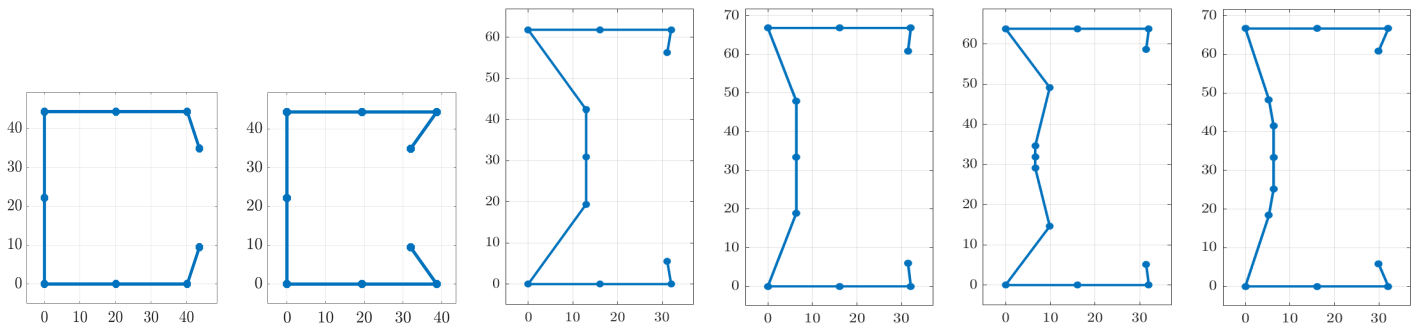

(a) 4-SA **(b)** 4-GA **(c)** 6-SA **(d)** 6-GA **(e)** 8-SA **(f)** 8-GA

Fig. 14. 64 mm stud optimisation results, $k_y = 20$ N/mm

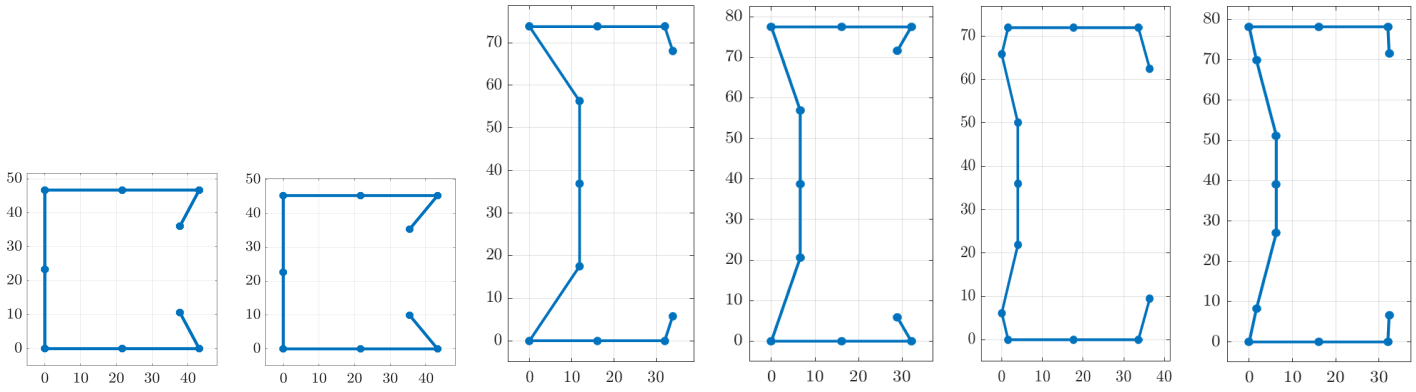

(a) 4-SA **(b)** 4-GA **(c)** 6-SA **(d)** 6-GA **(e)** 8-SA **(f)** 8-GA

Fig. 15. 76 mm stud optimisation results, $k_y = 20$ N/mm

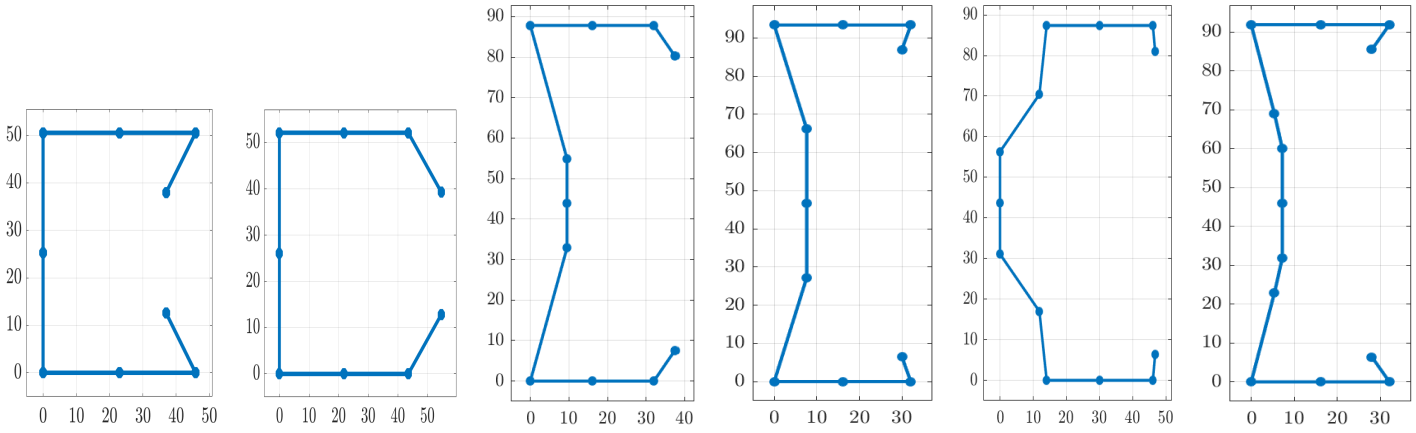

(a) 4-SA **(b)** 4-GA **(c)** 6-SA **(d)** 6-GA **(e)** 8-SA **(f)** 8-GA

Fig. 16. 92 mm stud optimisation results, $k_y = 20$ N/mm

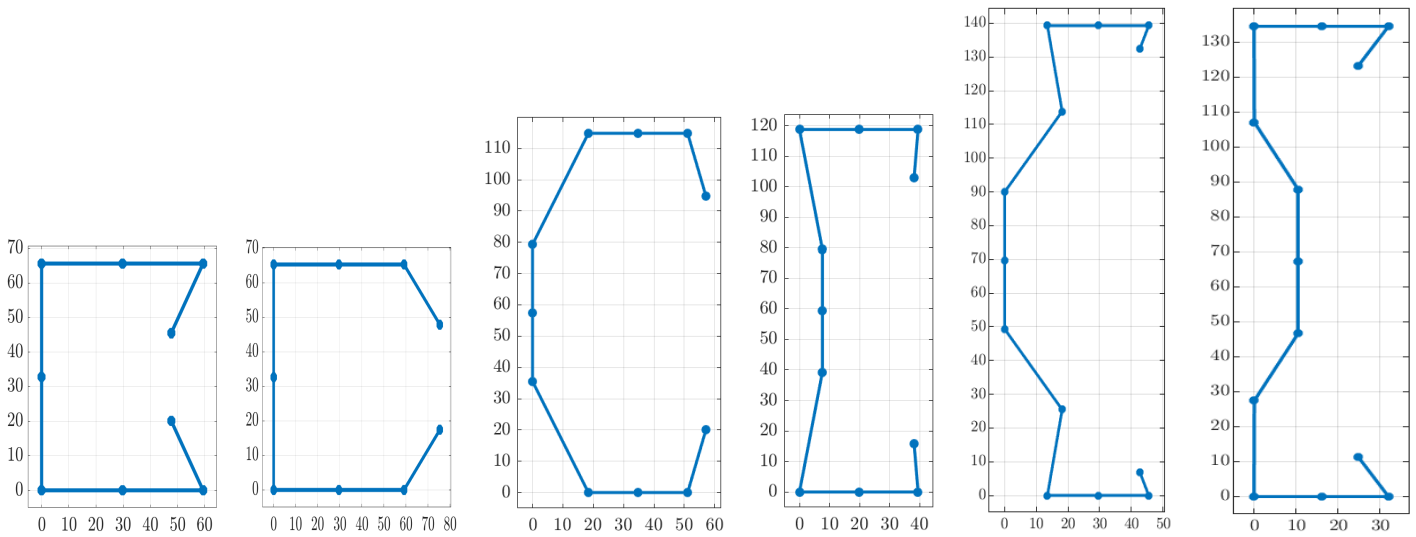

(a) 4-SA **(b)** 4-GA **(c)** 6-SA **(d)** 6-GA **(e)** 8-SA **(f)** 8-GA

Fig. 17. 150 mm stud optimisation results, $k_y = 20$ N/mm

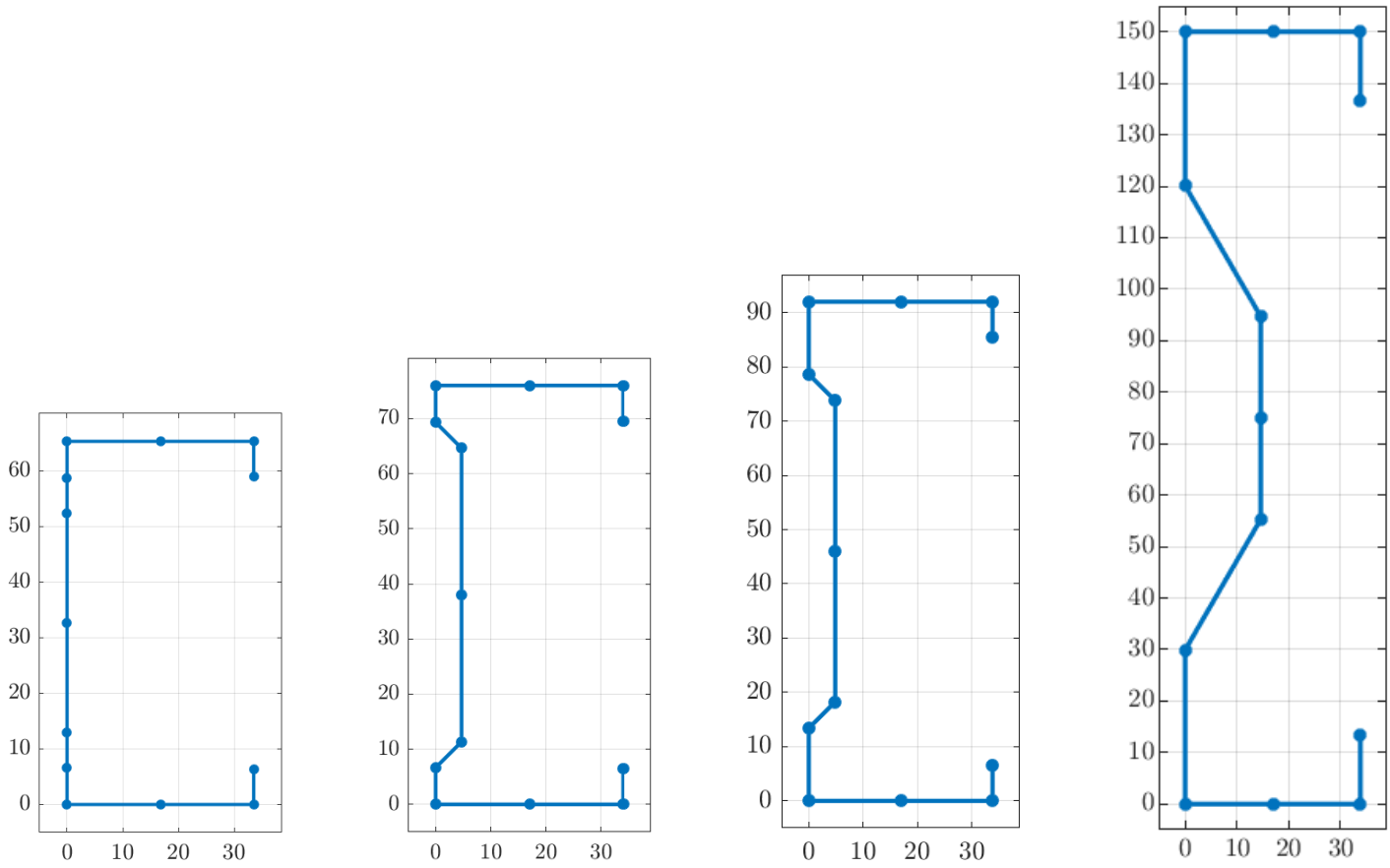

(a) 64 mm stud **(b)** 76 mm stud **(c)** 92 mm stud **(d)** 150 mm stud

Fig. 18. Depth constrained optimised sections

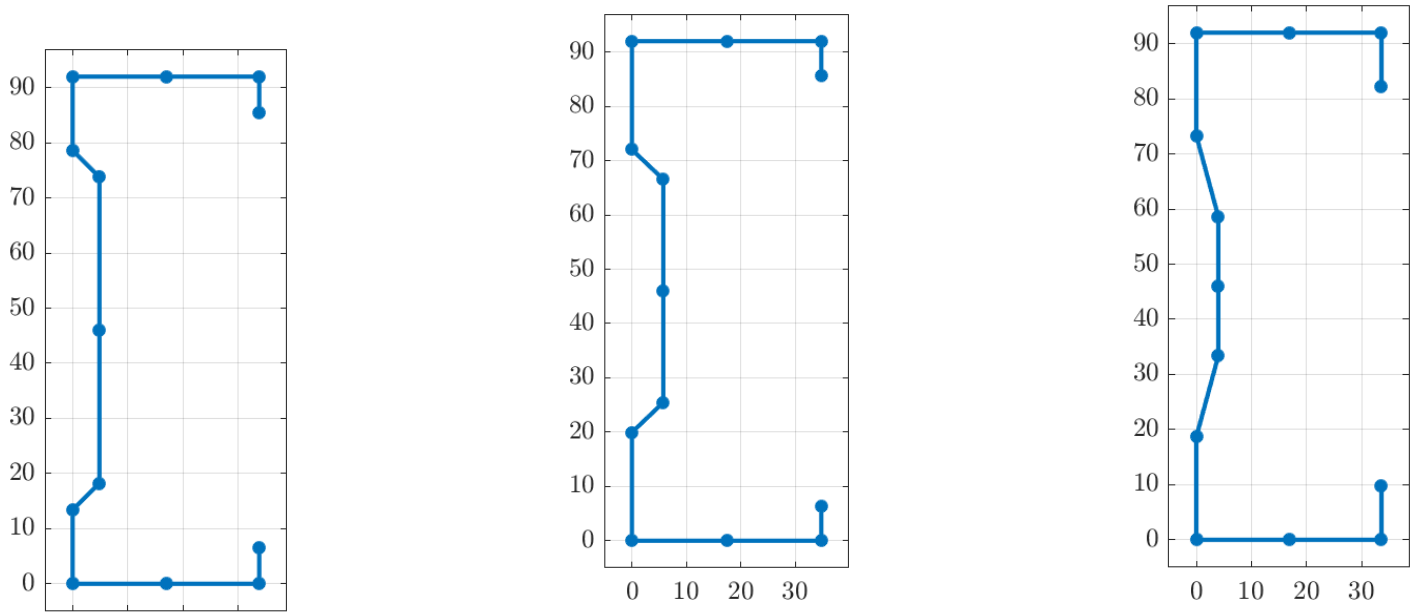

(a) No k_y restraints **(b)** 10 N/mm k_y restraints **(c)** 20 N/mm k_y restraints

Fig. 19. 92 mm depth constrained section optimisation with varying k_y restraints

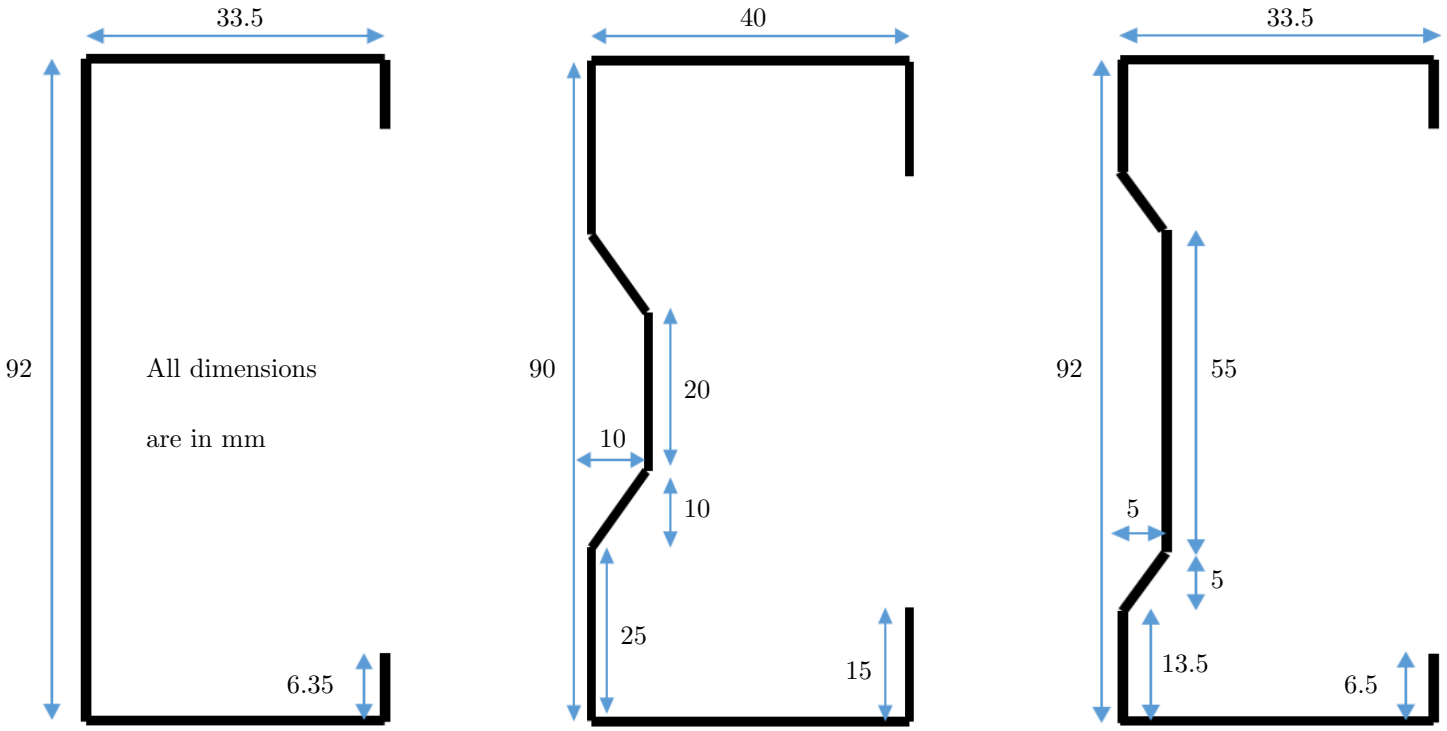

(a) 92 mm basic section **(b)** 90 mm web-stiffened section **(c)** 92 mm optimised section

Fig. 20. Comparison of performance of 92 mm sections

Table 1

1.15 mm basic section details

Basic section dimensions (mm)						Area (mm^2)
Description	BMT	Section depth	Flange width	Lip length	Strip length	
Web-Stiffened Stud	1.15	90	40	15	191	219.61
Basic Section	1.15	64	35.5	5	145	166.75
Basic Section	1.15	76	35.5	5	157	180.55
Basic Section	1.15	92	35.5	5	173	198.95
Basic Section	1.15	150	35.5	5	231	265.65

Table 2

Summary of optimisation results - $k_y = 0$

Original section depth (mm)	No of rollers	Optimisation scheme	f_{ol} (MPa)	f_{od} (MPa)	f_{oc} (MPa)	N_c (kN)	N_c/N_y	% increase in N_c
64	Basic section		339	302	171	25	0.25	
	4	SA	282	305	202	29	0.29	16
		GA	282	303	202	29	0.29	16
	6	SA	292	331	200	29	0.29	17
		GA	405	289	201	29	0.29	17
	8	SA	418	296	200	29	0.29	16
		GA	316	244	201	29	0.29	17
76	Basic section		245	262	232	33	0.30	
	4	SA	209	255	265	34	0.31	4
		GA	208	225	266	34	0.31	4
	6	SA	387	228	265	42	0.38	26
		GA	387	234	264	42	0.38	26
	8	SA	385	319	262	42	0.38	25
		GA	400	254	262	41	0.38	25
92	Basic section		170	204	325	40	0.33	
	4	SA	155	213	351	40	0.33	1
		GA	156	218	349	40	0.33	1
	6	SA	527	239	357	59	0.49	49
		GA	503	253	355	59	0.49	48
	8	SA	551	240	357	59	0.49	49
		GA	501	249	353	59	0.48	48
150	Basic section		65	74	754	42	0.26	
	4	SA	133	208	430	55	0.34	30
		GA	133	184	428	55	0.34	30
	6	SA	615	376	514	98	0.61	132
		GA	625	486	530	100	0.62	136
	8	SA	1054	524	729	114	0.70	169
		GA	713	513	709	113	0.70	167

Table 3

Summary of optimisation results - $k_y = 10$ N/mm

Original section depth (mm)	No of rollers	Optimisation scheme	f_{ol} (MPa)	f_{od} (MPa)	f_{oc} (MPa)	N_c (kN)	N_c/N_y	% increase in N_c
64	Basic section		339	304	535	52	0.51	
	4	SA	582	551	460	58	0.57	13
		GA	582	507	461	58	0.57	13
	6	SA	1005	413	562	65	0.63	25
		GA	643	455	556	64	0.63	24
	8	SA	1255	408	552	64	0.63	24
		GA	818	412	561	65	0.63	25
76	Basic section		245	263	569	51	0.46	
	4	SA	542	637	435	61	0.55	18
		GA	545	488	434	61	0.55	18
	6	SA	793	437	596	72	0.65	40
		GA	659	485	591	72	0.65	40
	8	SA	1206	431	586	71	0.65	39
		GA	916	437	592	72	0.65	40
92	Basic section		170	205	630	51	0.42	
	4	SA	455	450	418	62	0.51	22
		GA	454	440	419	62	0.51	22
	6	SA	681	469	642	82	0.67	60
		GA	743	486	649	82	0.67	60
	8	SA	1112	476	647	82	0.67	60
		GA	860	474	648	82	0.67	60
150	Basic section		65	74	985	42	0.26	
	4	SA	254	461	436	70	0.43	64
		GA	252	322	436	69	0.43	63
	6	SA	604	458	713	108	0.66	154
		GA	640	529	746	111	0.68	161
	8	SA	776	619	906	122	0.75	188
		GA	795	634	937	123	0.76	190

Table 4

Summary of optimisation results - $k_y = 20$ N/mm

Original section depth (mm)	No of rollers	Optimisation scheme	f_{ol} (MPa)	f_{od} (MPa)	f_{oc} (MPa)	N_c (kN)	N_c/N_y	% increase in N_c
64	Basic section		339	305	900	56	0.55	
	4	SA	602	501	817	70	0.69	24
		GA	616	599	816	70	0.69	25
	6	SA	1176	608	883	76	0.75	36
		GA	1194	626	908	77	0.75	37
	8	SA	1228	615	898	77	0.75	37
		GA	1170	625	908	77	0.75	37
76	Basic section		245	264	905	57	0.51	
	4	SA	532	538	770	72	0.65	27
		GA	545	521	765	72	0.65	27
	6	SA	903	610	887	83	0.75	46
		GA	917	623	907	83	0.75	47
	8	SA	1111	623	908	83	0.75	47
		GA	1085	621	910	83	0.76	47
92	Basic section		170	206	935	55	0.45	
	4	SA	458	567	722	74	0.61	35
		GA	456	465	726	74	0.61	35
	6	SA	1022	618	904	91	0.75	66
		GA	794	634	936	92	0.76	68
	8	SA	876	799	948	93	0.76	68
		GA	997	630	928	92	0.76	67
150	Basic section		65	74	1214	43	0.26	
	4	SA	267	529	636	80	0.49	88
		GA	269	346	631	80	0.49	88
	6	SA	575	505	928	112	0.69	163
		GA	644	562	973	117	0.72	175
	8	SA	801	699	1088	128	0.79	201
		GA	800	698	1072	128	0.79	200

Table 5

Depth constrained optimised stud details

Section depth (mm)	Basic section properties				Optimised section properties				
	Area (mm^2)	N_c (kN)	N_y (kN)	N_c/N_y	Area (mm^2)	N_c (kN)	N_y (kN)	N_c/N_y	A/A_{Basic}
64	166.75	25	102	0.25	166.75	26	102	0.25	1.00
76	180.55	33	110	0.30	184.87	37	113	0.33	1.02
92	198.95	40	121	0.33	203.26	56	124	0.45	1.02
150	265.65	42	162	0.26	290.59	125	177	0.71	1.09

Table 6

Results of 92 mm depth constrained optimised sections re-analysed without k_y restraints

Section's original k_y (N/mm)	Area (mm^2)	Revised k_y (N/mm)	N_c (kN)	N_y (kN)	N_c/N_y
0	203.26	0	56	124	0.45
10	206.34	0	56	126	0.45
20	206.70	0	57	126	0.45

Table 7

Comparison of the performance of 92 mm studs

Stud section	A_g (FSM/FEA) (mm^2)	FSM analysis		FE analysis results			
				Unsheathed		Sheathed	
		N_c (kN)	N_c/N_y	N_c(kN)	N_c/N_y	N_c (kN)	N_c/N_y
92 mm Lipped Channel	198.95/207.13	39.9	0.33	43.5	0.34	70.9	0.56
90 mm Web-stiffened Stud	219.61/232.91	55.8	0.42	66.7	0.47	101.7	0.72
92 mm Optimised Section	203.26/197.36	55.6	0.45	59.5	0.49	87.8	0.73